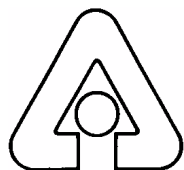


Chemical Technology
Division
Chemical Technology
Division
Chemical Technology
Division
Chemical Technology
Division
**Chemical Technology
Division**
**Chemical Technology
Division**
**Chemical Technology
Division**
Chemical Technology
Division
Chemical Technology
Division

Batch Tests with Unirradiated Uranium Metal Fuel Program Report

by M. D. Kaminski



Argonne National Laboratory, Argonne, Illinois 60439
operated by The University of Chicago
for the United States Department of Energy under Contract W-31-109-Eng-38

Chemical Technology
Division
Chemical Technology
Division
Chemical Technology
Division
Chemical Technology
Division

Argonne National Laboratory, with facilities in the states of Illinois and Idaho, is owned by the United States Government and operated by The University of Chicago under the provisions of a contract with the Department of Energy.

DISCLAIMER

This report was prepared as an account of work sponsored by an agency of the United States Government. Neither the United States Government nor any agency thereof, nor The University of Chicago, nor any of their employees or officers, makes any warranty, express or implied, or assumes any legal liability or responsibility for the accuracy, completeness, or usefulness of any information, apparatus, product, or process disclosed, or represents that its use would not infringe privately owned rights. Reference herein to any specific commercial product, process, or service by trade name, trademark, manufacturer, or otherwise, does not necessarily constitute or imply its endorsement, recommendation, or favoring by the United States Government or any agency thereof. The views and opinions of document authors expressed herein do not necessarily state or reflect those of the United States Government or any agency thereof, Argonne National Laboratory, or The University of Chicago.

Available electronically at <http://www.doe.gov/bridge>

Available for a processing fee to U.S. Department of Energy and its contractors, in paper, from:

U.S. Department of Energy
Office of Scientific and Technical Information
P.O. Box 62
Oak Ridge, TN 37831-0062
phone: (865) 576-8401
fax: (865) 576-5728
email: reports@adonis.osti.gov

ANL-01/33

ARGONNE NATIONAL LABORATORY
9700 South Cass Avenue
Argonne, IL 60439

**Batch Tests with Unirradiated Uranium Metal Fuel
Program Report**

By

M. D. Kaminski

Chemical Technology Division

December 2001

TABLE OF CONTENTS

	<u>Page</u>
ABSTRACT	1
I. INTRODUCTION AND BACKGROUND.....	1
Objectives.....	6
II. EXPERIMENTAL AND TECHNICAL APPROACH.....	6
III. RESULTS.....	11
A. UUBT1	12
1. Physical Observations	12
2. Gas Generation	14
3. Colloids	15
B. UUBT2	16
1. Physical Observations	16
2. Gas Generation	20
3. Colloids	20
C. Oxidic Testing	24
IV. DISCUSSION	25
V. FUTURE WORK	27
VI. ACKNOWLEDGEMENTS	27
VII. REFERENCES.....	28
APPENDICES.....	30
A. Raw Data and Measurement Tables.....	30
B. TEM Reports	38

LIST OF FIGURES

	<u>Page</u>
1. Oxidation Rate of Metallic Uranium as a Function of Oxygen Partial Pressure	2
2. Experimental Test Components	9
3. Controlled Atmosphere Containment Box Developed for Metallic Uranium Batch Testing Program.....	10
4. Measured O ₂ Concentrations in the Controlled Atmosphere Containment Box as a Function of Time Following Opening of the Gloveport.	11
5. Spallation Products from the Corrosion of Metallic Uranium Fuel after 45 Days.....	14
6. The Inferred H ₂ Gas Produced during the Corrosion of 98.4 mg of Uranium Metal in Test UUBT1	15
7. Optical Microscopic Image of the Partially Oxidized Fuel and Spalled Products Found at the Bottom of the Test Vessel	17
8. SEM Images of Suspended Uranium Oxides Found in Test UUBT2 at 55 Days.....	17
9. X-ray Diffraction Pattern for Oxidized Uranium Metal in EJ-13 at 90°C.....	19
10. The Inferred H ₂ Gas Produced during the Corrosion of 84.1 mg of Uranium Metal in Test UUBT2.....	20
11. Dissolved and Colloid Uranium Concentrations in Solutions from Test UUBT2	21
12. TEM of Two Types of Colloids Found during Test UUBT2.....	23
13. Transmission Electron Micrographs of Calcium-Rich Colloids Collected at 115 Days under Oxidic Conditions in Test UUBT2	25

LIST OF TABLES

	<u>Page</u>
1. Reaction Rates for Uranium Oxidation under Various Conditions.....	6
2. Elemental Concentration for Deaerated EJ-13 Water Used in the Mock Tests	7
3. Batch Test Information.....	13
4. Light Scattering Intensity for Samples Withdrawn during Test UUBT1.....	16
5. Diffraction Peaks Identified for Oxidized Uranium Metal	18
6. Measured Light Scattering Intensity for Samples Withdrawn during Test UUBT2	22
A1. Raw ICP-MS Data as Received from Analysis Report RFA# I-010104-1	31
A2. Raw ICP-MS Data as Received from Analysis Report RFA# I-010327-3	32
A3. Raw ICP-MS Data as Received from Analysis Report RFA# I-010327-3	33
A4. Raw ICP-MS Data as Received from Analysis Report RFA# I-010620-1	34
A5. Test Vessel Pressure Measurements Used to Estimate Uranium Oxidation Rates for Test UUBT1.....	35
A6. Test Vessel Pressure Measurements Used to Estimate Uranium Oxidation Rates for Test UUBT2.....	35
A7. Analysis and Cell Parameters for X-Ray Diffraction of Oxidized Uranium Metal from Test UUBT2 Day 108	36
A8. Analysis and Cell Parameters for X-Ray Diffraction of Silicon Powder Standard	37

ABSTRACT

Although the general environment of the proposed repository at Yucca Mountain is expected to be oxidizing in nature, the local chemistry within fuel canisters may be otherwise. The combination of low dissolved oxygen and corrosion of metallic fuels, such as Hanford's N-Reactor inventory, may produce reducing conditions. This condition may persist for periods sufficient to affect the corrosion and paragenesis of fuels and their reaction products. Starting in September 2001, unirradiated metallic uranium fuel was examined during batch tests under anoxic conditions. A series of tests carried out under inert atmosphere highlighted the rapid corrosion of the metallic uranium in EJ-13 water at 90°C. During the oxidation of the uranium, uranium dioxide fines spalled from the fuel surface generating copious amounts of colloids. The proportion of uranium-associated colloids accounted for nearly 50% to >99% of the uranium in solution after a brief period where no colloids were detected. The colloids were identified as individual (<10nm) and agglomerated uranium dioxide spheres as large as a few hundred nanometers in size. Silicate and alumino-silicate clays of diverse size and shape were also identified. The bulk size distribution as measured by dynamic light scattering was consistent with the microscopy observations in that the polydispersity indices were large, indicating a wide distribution of colloid particle sizes. The colloids were found to persist for periods beyond the scope of these tests and are at least partly stable. The anoxic experiments suggest that at least two mechanisms are responsible for uranium corrosion. The initial corrosion period is variably long but may last more than one month during which there is no net release of gas. Calculations of oxygen concentration in the vessel at the time of vessel closure show that this period is not consistent with the presence of dissolved oxygen, which would suppress H₂ production in undersaturated conditions. After this induction period, the fuel begins to produce H₂ gas until the coupon completely disaggregates into fine UO_{2+x} powder.

I. INTRODUCTION AND BACKGROUND

Although the general environment of the proposed repository at Yucca Mountain is expected to be oxidizing in nature, the local chemistry within fuel canisters may not be so. One can envision a scenario by which a fuel canister is breached thus allowing moisture to enter. Moisture reacting with metallic uranium fuels would deplete the available oxygen and may produce oxygen-starved conditions. These anoxic conditions may persist for periods sufficient to affect the corrosion and paragenesis of fuels and their corrosion products. The corrosion products are expected to come in contact with oxic conditions following their transport from the waste canister or potentially within the canister as a result of changing conditions. The changes brought about by the oxic front may be important.

It has been well documented that the rate of uranium metal corrosion (i.e., U→UO₂) is inversely dependent on the dissolved oxygen concentration and can accelerate by an order of magnitude at very low dissolved oxygen concentrations (see Fig. 1). Recently, we began

hydrologically unsaturated, drip testing of the irradiated uranium metal fuel (N-Reactor) in air and the results show that a significant quantity of colloids is generated during oxidation. It is unknown whether colloids would also be generated under reducing conditions and at what number density or rate. In addition, fission product and actinide disposition in an anoxic environment may be different from that in oxic tests.

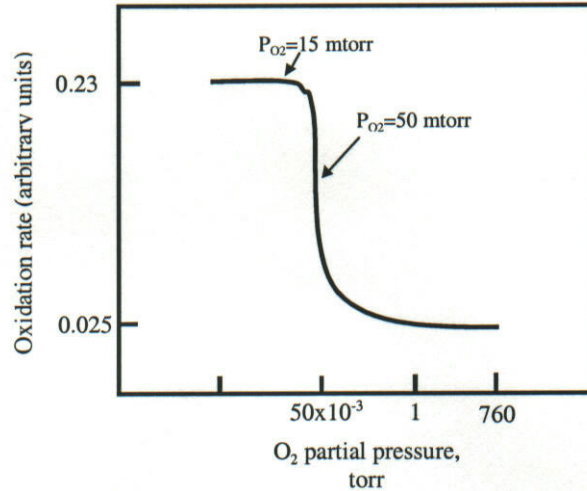
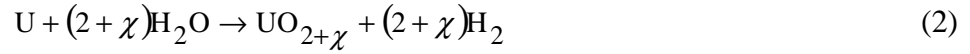


Fig. 1. Oxidation Rate for Metallic Uranium as a Function of Oxygen Partial Pressure [COLMENARES-1984]

Haschke summarizes the data [HASCHKE-1998] from a number of reviews on the oxidation characteristics of uranium metal. The oxidation of the surface is characterized by two distinct stages where the corrosion is limited by the diffusion of oxygen through the surface layer. The corrosion rate during the initial parabolic stage decreases as the thickness of the oxide layer grows. Following that, spalling of the oxide layer occurs and a constant effective layer thickness is achieved producing a linear rate of corrosion. The general corrosion rate R_U is quantified as

$$R_U = k \left(P_{O_2} \right)^m \left(P_{H_2O} \right)^n e^{\left(-E_a/RT \right)} \quad (1)$$

where k is the rate constant, m and n are empirical constants, P is the pressure, R is the gas constant, and E_a is the energy of activation. In general, m is negative and n is positive; thus under most conditions, O₂ and H₂O compete to suppress and enhance the corrosion of the metal, respectively. Of note, at low oxygen pressures ($P_{O_2} < 15$ mtorr or 20 ppm), $m=0$ and the rate is dependent only on the H₂O pressure. Under humid conditions at 100 °C, the uranium metal surface will be saturated with sorbed water and R will be independent of water pressure or $n=0$. Under oxygen-free conditions the spalled products are large flakes free of hydride and determined to be UO₂ and UO₃·H₂O [HASCHKE-1998]. This disagrees with Ritchie's results [RITCHIE-1981], which state that oxygen is needed for trioxide formation. The overall reactions for wet oxidation in the absence of oxygen is expressed as,

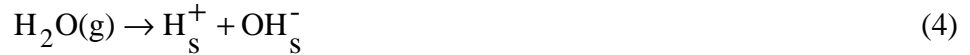


and with oxygen present,



where $\chi < 0.25$. Oxidation in dry atmosphere produces strongly adherent black films, while wet oxidation produces a fine, loose black powder. Wet oxidation in the presence of O_2 produces sheets of oxide that spall off once a critical thickness is reached ($\sim 1 \mu\text{m}$). Baker et al. [BAKER-1966] showed that oxygen concentration decreases linearly with time and that almost no H_2 is produced until all the oxygen is consumed. They postulated that uranium hydride (UH_3) formed during anoxic corrosion in a closed system, which explained the slight decrease in H_2 detected during experimentation.

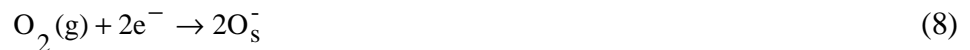
The role of water in Eq. 2 needs clarification. Many researchers have tackled the problem of mechanistically determining uranium oxidation in undersaturated conditions ($< 90\%$ relative humidity). Baker et al. [BAKER-1966] argued that wet oxidation in the absence of oxygen follows a mechanism by which hydroxyls are formed at the oxide surface (OH_s^-) and diffuse into the lattice, converting uranium into its oxide as follows,



The fate of the hydrogen radicals may involve hydrogen gas generation or hydride formation.



When oxygen is present, the reaction rate is reduced because of parasitic adsorption of O_2 onto reaction sites on the corroding uranium. The O_2 in this model converts hydrogen species produced by Eqs. 4 and 5 into water in an overall reaction,





Colmenares [COLMENARES-1984] explains that the reactants in the oxidation of uranium can be described by chemisorption and dissociation of water as follows:



and



where l and i are lattice-positioned and interstitial-positioned oxygen, respectively, in the UO_{2+x} lattice and O^- is derived from the catalytic breakdown of surface OH^- . The hydroxyl ions diffuse through the lattice in an interstitial mechanism and are responsible for the redox reactions with U^{4+} to produce the oxide much like in Baker's model:



The hydrogen is free to diffuse through the oxide, combine with another proton, and produce H_2 gas. This mechanism can explain the low activation energy for metallic uranium oxidation because of the relative ease with which OH^- and O^- can diffuse through a fluorite UO_2 lattice-type. Also, inhibition of corrosion by the presence of O_2 can be explained by its occupation of sites normally utilized by H_2O to produce hydroxyl ions.

McGillivray et al. [MCGILLIVRAY-1994] used secondary ion mass spectrometry (SIMS) and argues that the uranium oxidation rate can be explained via a Langmuir-type model above ~ 150 °C:

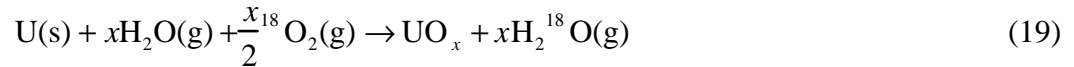
$$R_U = \frac{k_1 P_{\text{H}_2\text{O}}}{1 + k_2 P_{\text{H}_2\text{O}}} + D \quad (14)$$

where k_1 and k_2 are the rate constants related to the sorption and desorption, $P_{\text{H}_2\text{O}}$ is the vapor pressure of water, and D is the dry air oxidation rate. This expression predicts a plateau in the oxidation rate as $P_{\text{H}_2\text{O}}$ is increased ($R_U = k_1/k_2 + D$ as $P_{\text{H}_2\text{O}} \rightarrow \infty$) and is only applicable to relative humidity below 90%. Oxygen occupies available sites on the UO_2 lattice and contributes to the oxidation of uranium by introducing O^{2-} species, which diffuse more slowly than water-derived hydroxy species (identical to dry oxidation of uranium). Hydrogen bonding allows water to adsorb on top of the chemisorbed O_2 layer and continue to react with the surface, albeit at a lower rate. So, both H_2O vapor and O_2 are believed to contribute reacting species so that the rate is $\sim 75\%$ from H_2O -contributing species and $\sim 25\%$ from O_2 -contributing species at 100 °C in moist air.

Haschke [HASCHKE-1998] recently suggested that the reaction proceeds via the following mechanism by which oxygen is separated from water:

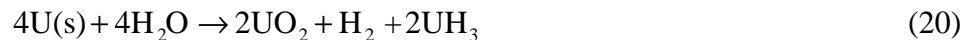


where (ads) indicates species adsorbed to the UO_2 lattice. Baker and Haschke mechanisms are consistent with isotope-labeled ^{18}O experiments of Baker et al. [BAKER-1966] for a net reaction of



where the ^{18}O is traced. Weirick [WEIRICK-1984] did not substantiate the isotopic studies of Baker et al. [BAKER-1966], but Haschke [HASCHKE-1998] dismissed Weirick's results because of a number of inconsistencies. In support of Weirick, McGillivray's mechanisms allows for isotopically rich and normal oxygen to appear in the oxide simply because both gases, O_2 and H_2O , impart reacting species (O^{2-} and OH^- , respectively). It is clear that more careful work is needed in the use of isotopically labeled H_2O and O_2 before a conclusion can be drawn.

Above 90% RH, the reaction rate again changes, indicating a change in reaction mechanism. Saturated vapor conditions yield equivalent corrosion rates to water immersion tests [BAKER-1966] when no O_2 is present in either system. Increasing humidity above 50-70% (greatly depending on test sample) will produce a maximum in oxidation rate that can then lead to a reduced rate at humidity levels approaching saturation. Baker et al. [BAKER-1966] explained that this could be due to water invasion into microfissures in the oxide layer that suppress the release of H_2 . The buildup of H_2 in the microfissures simultaneously slows water diffusion to the oxide-metal interface that reduces the corrosion rate at levels approaching saturation. If oxygen is present, the rate increases markedly near water saturation and may be explained by surface pitting and the exclusion of O_2 from surface sites by the mass action of water, both phenomena increasing the availability of water to react with the metal. Hydrogen is produced at a linear rate in accordance with the mechanism of Eq. 2 with slightly less than stoichiometric H_2 (>85%). The deficit is owed to UH_3 production that reduces H_2 generation by a factor of eight¹ via



¹Compare to Eq. 2 where 2 H_2 are produced for every U oxidized.

Typical rates determined for the corrosion of uranium metal are provided in Table 1 for reference.

Table 1. Reaction Rates for Uranium Oxidation under Various Conditions

Author	P_{O_2}	RH (%)	T	Rate (mg/cm ² /h)
ORMAN-1964	0	100	100	4.75
ORMAN-1964	0	immersed	100	4.2
WABER-1952	0	immersed	90	1.01
RITCHIE-1981	0	100	90	1.54
WABER-1952	air	immersed	80	0.57
RITCHIE-1981	air	100	90	0.09

In the case of irradiated fuels, it has been shown that the corrosion rate was not enhanced due to radiolysis products as demonstrated during gamma irradiation experiments [BAKER-1966]. Instead, the small increase in reaction rate with irradiated fuel results from a decrease in fuel density and increase in swelling.

Objectives

The objectives of the batch tests with metallic uranium fuel was to determine the effects of an anoxic environment on the corrosion of metallic uranium fuels by assessing the paragenesis of alteration products, disposition of fission products and actinides, colloid occurrence and properties, and solution chemistry. Following this anoxic testing period, the fuel was exposed to oxidic conditions and the immediate change in solution chemistry and paragenesis assessed.

II. EXPERIMENTAL AND TECHNICAL APPROACH

The experimental procedure is detailed in the Standard Operating Procedure – Procedure for Batch Testing of Metallic Uranium Fuel Under Saturated Water and Variable-Oxygen Atmosphere (WMRD-SOP-061, Rev. 0) but will be paraphrased here. Scientific Notebook #1763 contains all data or references to data generated under this program.

All tests were run in 22-mL stainless steel Parr vessels. The Parr vessel caps were modified with welded quick-disconnect male fittings to accept a gas pressure gauge. Water from the J-13 well was reacted at 90 °C for 21 days with crushed core samples of Topopah Spring tuff. J-13 well water prepared in this manner is called EJ-13 and is characterized by a higher silicon and sodium content than J-13 water. Ultrapure nitric acid (16 M) was used to acidify samples prior to analysis (~5 μ L per 400 μ L sample). EJ-13 (MG Bottle #3 or TSR#MK09) was purged with humid N₂ for 1.5 days before initial use and stored in the anoxic atmosphere thereafter. All components were purged with Ar or N₂ before use. By measuring the dissolved oxygen, it was observed that sparging the solution with N₂ or Ar gas reduced the dissolved oxygen concentration within about one minute to below the detection limits of the probe (0.04 ppm). By providing a blanket of inert gas (as opposed to sparging the solution by submerging the gas line in the solution) the O₂ can be reduced to <0.04 ppm in about 20 min. Water from MG Bottle #3

was used for the initial experiment (test UUBT1) and stored in the portable glovebox (atmospheric O₂ was 1.9-2.3%). Water from TSR #MK09 was stored in the Plexiglas containment box (atmospheric O₂ < 10 ppm). See below for descriptions of the glovebox and containment box configuration. The EJ-13 batches were analyzed regularly and typical values are shown in Table 2.

Table 2. Elemental Concentration for Deaerated EJ-13 Water Used in the Mock Tests

Element	Conc., ng/g	Standard Deviation	Element	Conc., ng/g	Standard Deviation
Li	70	70	Fe	800	400
B	80	300	Zr	2	1
Na	46000	6000	Au	<2.6	0.8
Mg	300	100	U	<1.8	0.5
Al	500	300	Ni	9	6
Si	35000	3000	Sr	39	2
P	380	70	Cs	1.8	0.3
K	10000	2000	Np-237	<0.1	<0.1
Ca	8400	700	U-238	0.6	0.6
Cr	<45	20	Pu-239	<0.2	<0.2
Mn	<8	2	Am-241	<0.1	<0.1

All activities were done in the controlled atmosphere except where noted and during the oxic testing periods (see below). The fuel was cut from unirradiated N-Reactor fuel elements into small wedges with the cladding removed. The fuel was polished with 600 grit SiC and ultrasonically rinsed in deionized water for 2-3 min. The test was initiated by placing the fuel piece (~100 mg) at the bottom of the Parr vessel or on a gold screen (11- μ m nominal opening) held in a steel lifting bail. The EJ-13 was added to the vessel (10-16 mL), the vessel was sealed to 140 ft-lb torque with steel enclosures and a copper gasket, and placed in the heating block at 90°C until it was sampled. A test vessel were sampled by cooling the vessel to room temperature using dry ice, transferred out of the glovebox (for UUBT1) and weighed, and the cap was loosened but not fully opened (test UUBT2 was located outside the containment box when sealed). The vessel was transferred back into the glovebox or containment box, the cap was removed, pictures were taken, and liquid samples were withdrawn for analysis. Four hundred microliters each was withdrawn for pH measurement, dissolved ion concentration (by passing through a 30,000 MW filter), colloid + dissolved ion concentration² (by passing through a 0.45 μ m filter), and the colloid size distribution. Tests were restarted, following a sampling, by resealing the vessel and replacing it in the heating block or replenishing the EJ-13 volume in the vessel before sealing.

Pictures were captured by a digital camera, alone, or attached to a Navitar (12X) zoom lens optical microscope. Field of view was measured with a mechanical ruler. Solutions were

²By subtracting the dissolved ion filtrate concentration from this value the uranium concentration associated with colloids is determined.

submitted to in-house inductively coupled plasma-mass spectrometry (Fisons VG PlasmaQuadII+ series) as described elsewhere [WOLF-1998]. The Eh was measured with a ORION 420A combination pH/Eh instrument and Pt-Ag/AgCl electrode. Solution pH was measured with a Sentron Instruments 2001 pH meter. Electron microscopy was performed by passing 5 μ L of solution through a holey carbon grid and analyzing the grid using a Hitachi S3000N scanning electron microscope (SEM) coupled to a NORAN energy dispersive X-ray spectroscope (EDS), and a JEOL 2000 FXII transmission electron microscope operating at 200 kV. Dissolved oxygen was measured using a Microelectrodes, Inc. Model MI-730 O₂ selective electrode and OM-4 oxygen meter calibrated to deionized water equilibrated with ambient air. The dissolved oxygen was computed based on the instrument readout according to Eq. 20:

$$CO_2[\text{ppm}] = \frac{a}{22.414} \frac{(760 - p)}{760} \frac{R}{100} \times 32 \times 1000 \quad (21)$$

where R is the universal gas constant, a is a temperature-dependent constant (0.03044 at 21 °C) and p is the pressure in mm of Hg (18.65 at 21 °C). Solutions in equilibrium with the atmosphere show a reading of 20.9 or 8.86 ppm. The detection limit for this instrument is 0.04 ppm dissolved oxygen or 0.1% O₂ in gas. The containment air was monitored using a Teledyne Analytical Instruments AO 316-H oxygen analyzer calibrated to ambient air.

Colloid size distribution was estimated using photon correlation spectrometry or dynamic light scattering [Malvern PCS4700C analyzer and Uniphase Ar ion laser (Model 2213-75CL)] checked against NIST polystyrene standards (SRM 1963 and SRM 1691, 100 and 300 nm nominal diameters, respectively). Colloid samples were withdrawn from the test vessels into cylindrical glass vials and capped. Samples were stored in the reservoir of the containment box at room temperature and purged continuously with N₂.

Before exposing the test vessels to an oxic environment, a small amount of oxidized fuel slurry powder (<5 mg) was removed by pipette for XRD analyses. This sample was stored in the containment box until removed for analysis. The estimated exposure time of fuel powder to ambient air was <2 h, for sample preparation and transfer, and 24 h for analysis. This time is not considered sufficient to cause further oxidation of the fuel powder. The sample was prepared by centrifuging the wet powder and withdrawing the supernatant EJ-13. Ethanol was added to the vial, and the resultant suspension withdrawn by pipette onto a zero-background single crystal silicon XRD planchet. The ethanol was driven off by placing the planchet in an oven at 90 °C for five minutes. The ethanol provided a suitable fixing agent for this type of powder sample. The solid products were identified using a Rigaku MiniFlex X-ray diffractometer, and the results compared to powder diffraction files from the International Centre for Diffraction Data. Standard silicon powder was analyzed subsequent to the sample analysis to check calibration and was in full agreement. (See Appendix A for the raw data and diffractometer scan parameters.)

An anoxic environment was created for test sampling and restarts. It was designed to provide adequate radiation shielding for eventual tests with irradiated metallic uranium fuels. The initial experimental setup for the anoxic test conditions was created in a portable glovebox purged with Ar or N₂ (see Fig. 2). The glovebox was modified to include a temperature-

controlled aluminum block capable of single-temperature control of four to six vessels (22- or 44-mL Parr vessels). A Parr vessel filled with sand was connected to the external power supply via two thermocouples to control the block temperature and for over-temperature control. The glovebox was purged with dry Ar daily, but not continuously. Samples and supplies were transferred in and out of the glovebox in a manner minimizing oxygen invasion. Equipment was first placed in the transfer port with the inner door sealed. The transfer port was evacuated to -15 psig, filled with dry Ar to -5-0 psig, evacuated to -15 psig, and filled again with dry Ar to 0 psig. The contents were then transferred through the inner port to the glovebox. Transfers outside the glovebox were completed by opening the inner port (the transfer port was filled with Ar from the previous transfer), placing the contents into the transfer port, and closing the inner port. The outer port could then be opened to remove the contents.

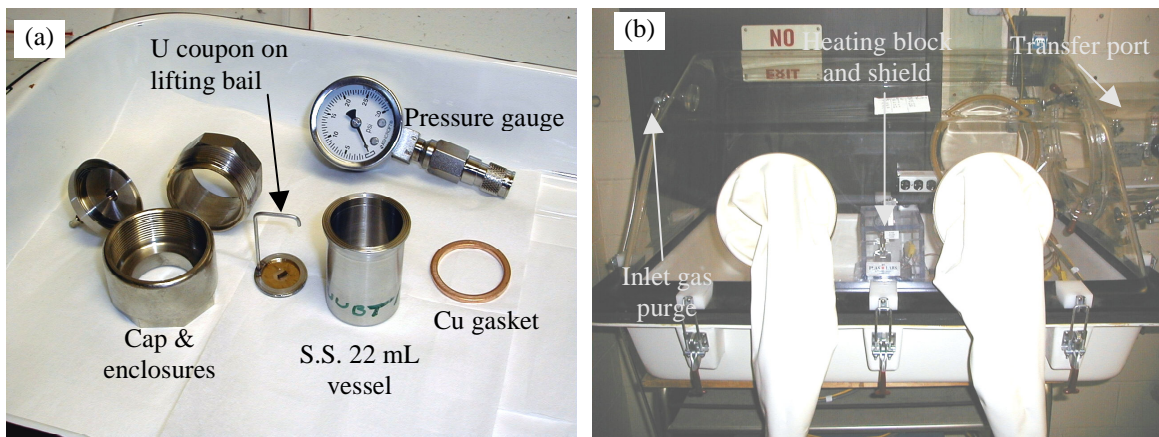


Fig. 2. Experimental Test Components: (a) Batch Test Vessel and Components and (b) Portable Glovebox Used in Anoxic Uranium Metal Batch Tests

It was recognized during the mock test UUBT1 that there were several deficiencies in the experimental setup. First, the oxygen concentration in the glovebox was consistently 1.8-2.0 mol% O₂ at 21°C. The dissolved oxygen for a solution in equilibrium with the glovebox gas at this O₂ level is 0.76-0.85 ppm. The dissolved oxygen that was measured in the EJ-13 stock bottle (MG Bottle #3) was 2.3% or 0.98 ppm. These levels were not considered sufficiently low to eliminate the participation of oxygen in the corrosion of the fuel.

Before the start of the second mock test UUBT2, the experimental setup was modified to address the aforementioned concerns. A Plexiglas containment box was fabricated for operation within a standard fume hood. As shown in Fig. 3, the containment box contained an air pump for continuous sampling of the O₂ levels in the box, a working platform, cylindrical access shaft in the top (not shown) for a digital microscope, and storage unit below. A trap door in the floor of the working platform allowed access to vials in the storage unit. The entire containment box was purged constantly with N₂ that had been filtered to remove oils and moisture. The joints in the Plexiglas were sealed with RTV except for the top that was rendered tight by placing a rubber gasket between it and the tops of the six walls and sealing with screws. For this setup, the containment box O₂ levels were monitored using the Teledyne O₂ Analyzer because the O₂ levels would be below the detection limit of the O₂ selective electrode.

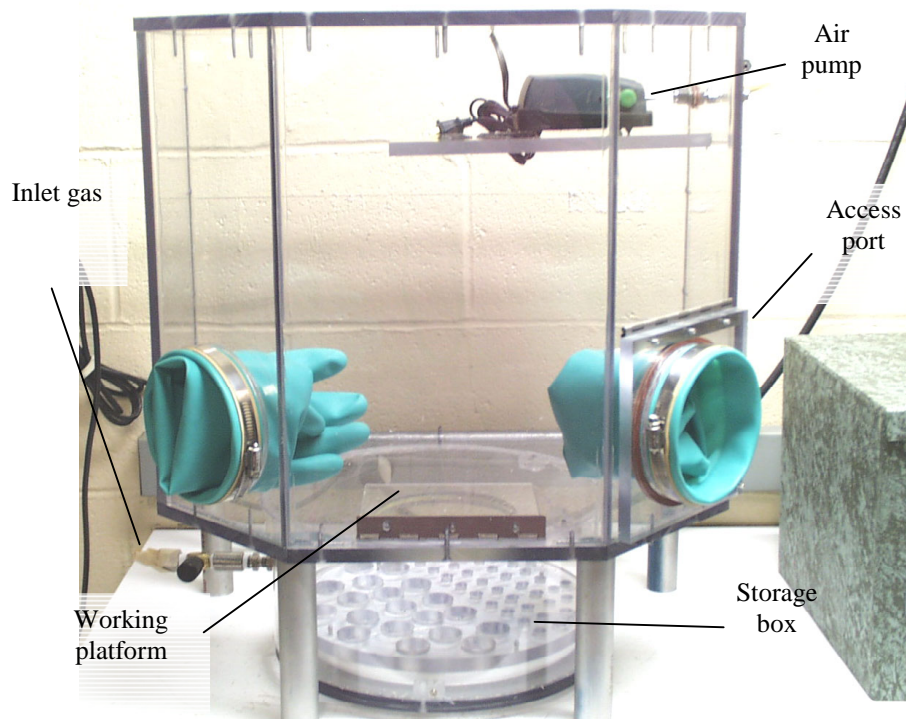


Fig. 3. Controlled Atmosphere Containment Box Developed for Metallic Uranium Batch Testing Program

The O_2 levels were measured in the containment box to simulate real preparation and sampling conditions. The box could maintain <50 ppm O_2 in N_2 during active sampling and <10 ppm when the box was left undisturbed. Inserting items into the containment box required entrance through the gloveport, which introduced atmospheric oxygen into the box. Figure 4 contains plots of the oxygen levels in the box after opening the gloveport at various N_2 inlet purge pressures. As can be seen, the containment box is purged quickly: only 20 min is required to reach <10 ppm from initial levels of 11,000 ppm.

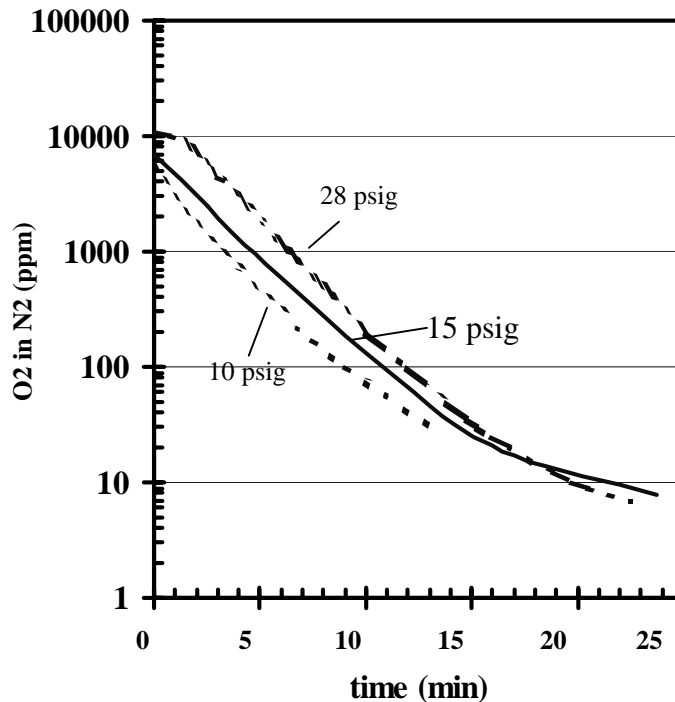


Fig. 4. Measured O_2 Concentrations in the Controlled Atmosphere Containment Box as a Function of Time Following Opening of the Gloveport. N_2 purge pressure was 10, 15, and 28 psig

III. RESULTS

The mock uranium batch test program schedule is highlighted below.

Safety review	Approved 9/00
Portable glovebox modified	Completed 9/00
Draft Test Plan Approval	9/00
UUBT1* Test Start:	9/22/00
UUBT1 Sampling:	9/28/00, 10/10/00, 10/24/00, 11/6/01
UUBB1 [†] Blank Test Start:	11/00
Test Plan	Approved 1/30/01
Standard Operating Procedure	Approved 2/12/01
UUBT2 [‡] Test Start:	1/25/01
UUBT2 Test Sampling:	1/31/01, 2/22/01, 3/20/01, 5/11/01, 6/11/01
UUBB1 Test Start:	2/22/01
UUBB1 Test Sampling	6/18/01

*Unirradiated Uranium Batch Test sample #1

[†]Unirradiated Uranium Blank Batch test #1

[‡]Unirradiated Uranium Batch Test sample #2

More details for the three tests UUBT1, UUBT2, and UUBB1 are given in Table 3 and the following sections will detail the individual tests, in turn. In the final section, a summary will be provided. The starting pH of the deaerated EJ-13 was 8.0-8.6, similar to the aerated values. For UUBT1 no EJ-13 was added to the test vessel at samplings to replenish any lost liquid. The liquid contents decreased from 15.99 g to 9.85 g at test termination due to aliquots removed for sampling and vapor lost at the lid/base closure seal. Tests UUBT2 and UUBB1 were replenished with EJ-13 to compensate for lost volume. For UUBT1, the pH of the reacted solution was slightly acidic at 5.8-5.9 while the blank pH was 7.1. The Eh of the EJ-13 before the test start was 240 mV (vs. Calomel) and was not significantly different than aerated EJ-13. The Eh was monitored periodically during test UUBT2 and was consistent with UUBT1 values.

A. UUBT1

1. Physical Observations

Test UUBT1 was first sampled after six days. The fuel was intact and black, but a small volume of black UO_2 fines was noted on the gold screen of the lifting bail. After 17 days, the proportion of fines increased and, now, mixed brown and black fines could be discerned. The fuel surface had browned noticeably but was not noticeably reduced in size. The brown color of UO_2 is consistent with near stoichiometric UO_2 ($x \rightarrow 0$), H_2 presence, and reducing conditions, although there was no evidence of appreciable gas generation until about 40 days into the test.

After 32 days, the population of brown colored fines immediately surrounding the fuel had increased. The fuel surface was brown with hints of black. Representative morphologies for the uranium fines are shown in Fig. 5. The fines appeared to be exfoliated sheets of the oxidized metal $<1 \mu\text{m}$ thick or flaky agglomerations that were typically $<30 \mu\text{m}$ in length. When the vessel was opened after 45 day, the fuel was ~80-90% disaggregated into brown fines.

Table 3. Batch Test Information

Test No.	Fuel Mass and SA	Test Description	Date	Initial Water,		pH	Water Lost, g	EJ-13 MG Bottle #	O ₂ Concentration
				g	Time, d				
UUBT1	0.0984g SA=23.2 mm ²	Test initiation	9-22-00	15.99	-	8.6	0	EJ-13	nm*
		Sampling 1	9-28-00	14.06	6	5.8	1.93-0.4 ⁺	#3	nm
		Sampling 2	10-10-00	12.06	17	5.9	0.17	Eh=240	nm
		Sampling 3	10-24-00	10.33	32	5.9	1.66		nm
		Sampling 4	11-6-00	9.85	45	nm	0.19		0.98 ppm in EJ-13, 0.81 in vessel
		Termination	12-11-00	nm		nm	nm		nm
UUBT2	0.0841g,	Test initiation	1-25-01	15.46	-	8.0		TSR# MK09	<15 ppm
		Sampling 1	1-31-01	14.17	6	nm	0.86		<10 ppm
		Sampling 2	2-22-01	13.56	28	8.0	0.32	Eh=223	<20 ppm
		Sampling 3	3-20-01	14.33	55	8.4	0.28		<10 ppm
		Sampling 4	5-10-01	16.78	107	water replenished	11.28		<15 ppm
		Sampling 5/Oxic initiation	5-11-01	15.89	108	7.73	2.35		<20 ppm/air
		Sampling 6/Oxic	6-11-01	16.04	115	8.04	0.12		air
UUBB1	no fuel	Test initiation	2-22-01	16.38	-	8.0		TSR# MK09	<20 ppm
		Sampling 1/Oxic initiation	6-18-01		116	7.1	1.65		<20 ppm/air

*Not measured.

⁺ Although water vapor was lost from the vessel due to a leaky gasket, the loss was not believed to be sufficient to offset the pressure buildup due to H₂ generation. This was confirmed in UUBT2 where water vapor losses were minimal during the pressure-monitoring period up to 55 days.

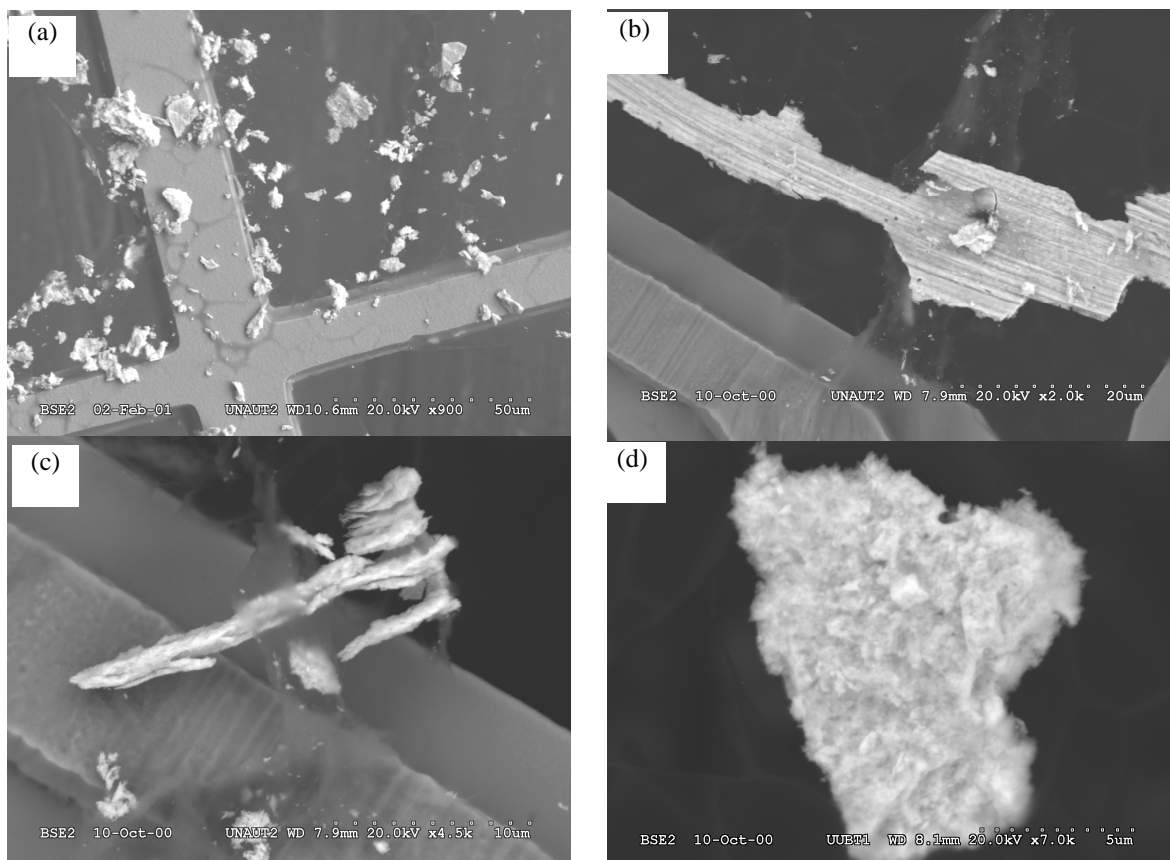


Fig. 5. Spallation Products from the Corrosion of Metallic Uranium Fuel after 45 days. (a) An expanded view. A closer view is provided of the exfoliated sheets (b, c) and the flaky surface of some fines (d). The test vessels were exposed to containment air with 2% O₂.

2. Gas Generation

Between sampling at 32 and at 45 days into the test, 2-3 psig of gas was generated in the vessel. The vessel was resealed after 45 days and the gas pressure rose linearly until about 66 days as shown in Fig. 6. Assuming the mechanism shown in Eq. 2 with $n=0$, the calculated uranium corrosion rate is 1.9 mg U/d for the linear period from 45-66 days. During this period the amount of fuel oxidized corresponded to 1.9 mg/d x 22 d = 41.8 mg or 42% of the fuel. If H₂ production were the preponderant mechanism, then approximately 52 days would be required for complete oxidation of the fuel at this rate, ignoring other effects (e.g., surface area, ionic transport). From this exercise, it is quite apparent that the fuel corrosion followed at least two mechanisms. The corrosion mechanism that dominated the initial period produced no measurable gas release for a period lasting almost one month. These results are completely contrary to those of Baker et al., as one would expect a linear rate of H₂ production in accordance with Eq. 2. Afterward, a net gas release was observed signaling a second mechanism and implying the dominance of Eq. 2. It also appears that since gas production began before a sampling (when the O₂ levels in the vessel would be most depleted)

and continued after the sampling, once the second period had begun it continued despite the solution being partly equilibrated with air containing 2% O₂. This behavior suggests that the onset of the second period is independent of the oxygen concentration in water and must therefore be a function of the altered matrix of the fuel. In other words, the fuel condition by about the 45th day had become such that hydrogen gas was not being suppressed, since its production is expected based on undersaturated tests, as described in the Introduction.

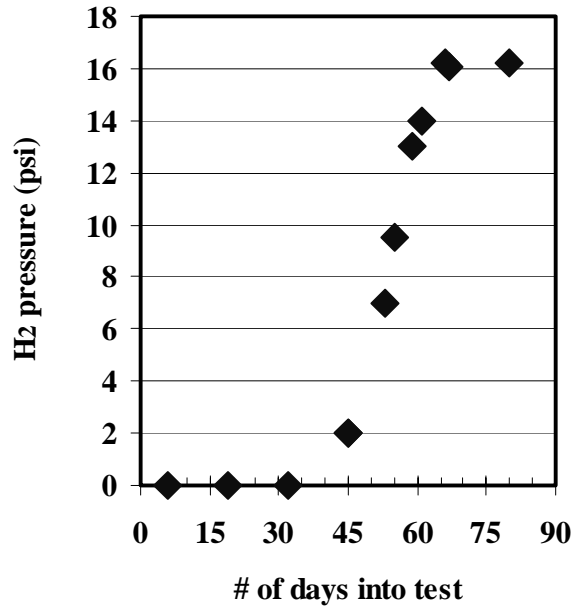


Fig. 6. The Inferred H₂ Gas Produced during the Corrosion of 98.4 mg of Uranium Metal in Test UUBT1

3. Colloids

Colloids were not present in detectable concentrations until the sampling at day 17. Table 4 provides supporting data. By day 6, the scattering intensity of the solution³ was comparable to that of deaerated EJ-13 water (~6-10x10³ counts/sec). By day 32 the dissolved uranium concentration had risen from 500 ppb at days 6 and 17 to 2660 ppb and a colloid population had formed to detectable concentrations producing scattering intensities ten times background. Analysis by ICP-MS could not confirm the existence of colloidal uranium by day 32, within the limit of the calculation error, nor could other elements typically observed in fuel environmental colloids be determined to reasonable accuracy (see Appendix A for compilation of ICP-MS data). Of course, this does not mean that the colloids detected by light scattering could not be composed of uranium, aluminum, or silicon, or other elements but that the subtraction technique used to determine colloid concentration is insufficiently accurate. In fact, as shown in the following section, the colloids borne from uranium corrosion are

³The light scattering intensity is a measure of the number of colloids in the sample assuming colloids of monomodal size are generated.

composed of many elements not apparent from solution elemental analysis. Size distribution data could not be generated by light scattering analysis due to the disperse nature of the sample indicated by the polydispersity index from light scattering analysis. The polydispersity for UUBT1 samples was typically >0.5 .⁴

Table 4. Light Scattering Intensity for Samples Withdrawn During Test UUBT1

Sample	Date of Analysis	Light Scattering Intensity ($\times 10^3$ cps)	Laser Power (mW)
EJ-13	periodically	6-10	3
day 6	10-11-00	60	50
day 17	6-26-01	22	3
day 32	11-6-00	100	3
day 32	6-26-01	<10	3

The stability of the colloids was examined by periodically analyzing stored samples. Light scattering intensities also are shown in Table 4 for the limited data set. Though colloids collected at day 17 (10-10-00) were analyzed 8 1/2 months later (6-26-01) and were readily detected, they were not detected in the day 32 sample analyzed nine months after collection. At this point, it is unclear whether the colloids are stable for transport or sensitive to slight changes in solution that may occur during storage or subsurface transport. Colloid stability is examined in more detail in the next section describing results from UUBT2.

B. UUBT2

1. Physical Observations

Because the O_2 concentration maintained in the glovebox used for Test UUBT1 was not sufficiently low (1.8-2.0 mol% O_2), a second test, UUBT2, was run in a containment box with significantly lower O_2 (<50 ppm O_2 in atmosphere). As in test UUBT1, the fuel in UUBT2 produced spalled products but remained in good condition with sharp edges and corners after six days. Up to day 55, the original fuel piece was distinguishable but the vessel bottom was dominated by UO_2 fines. After 108 days the fuel appeared to be completely converted to the UO_2 fines. The fines appeared to be similar in morphology to those examined from UUBT1 at test termination when less flaky particulate was abundant. Example micrographs are provided in Figs. 7-8. Baker et al. [BAKER-1966] reported that fines created under oxygen-starved conditions had a BET surface area of $30 \text{ m}^2/\text{g}$.

⁴A polydispersity index of <0.3 is ideal for light scattering although values as high as 0.5 have been amenable under special circumstances.

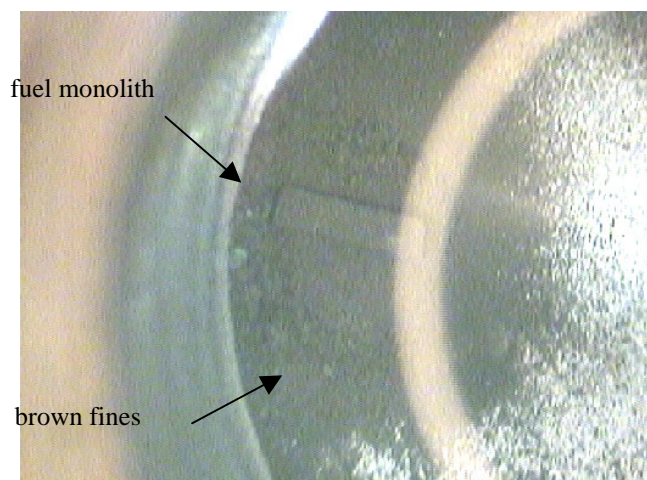


Fig. 7. Optical Microscopic Image of the Partially Oxidized Fuel and Spalled Products Found at the Bottom of the Test Vessel (Test UUBT2 at 28 Days, Field of View = 14.7 mm)



Fig. 8. SEM Images of Suspended Uranium Oxides Found in Test UUBT2 at 55 Days

A portion of the powder was collected for XRD analysis. The diffraction peaks for the sample collected after 108 days of reaction are shown in Table 5.

Table 5. Diffraction Peaks Identified for Oxidized Uranium Metal

Peak Location (2θ)	Relative Intensity	Full Width Half Maximum ($^\circ$)
12	3.3	0.12
28.447	100	1
32.799	38	1.075
47.365	47.1	1.319
56.031	37.9	1.319
58.722	8.5	1.319
69.011	4.8	1.825
76.114	13.4	1.825
78.411	8.9	1.825
87.926	9.8	2.04
94.665	8.4	2.04
~107	5.9	>2
~115	17.3	>2

The diffraction pattern is shown in Fig. 9 and reveals remarkably wide peaks, which correspond to very small scattering domains and this will be expounded on shortly. All peaks can be accounted for by uraninite except for that occurring at $2\theta=12.0^\circ$. The location of this peak is consistent with higher oxidation uranyl oxyhydroxides of which schoepite $(\text{UO}_2)_8\text{O}_2(\text{OH})_{12}(\text{H}_2\text{O})_{12}$ ($2\theta=12.001^\circ$), metaschoepite $(\text{UO}_2)_8\text{O}_2(\text{OH})_{12}(\text{H}_2\text{O})_{10}$ ($2\theta=12.041^\circ$), and possibly ianthinite $\text{U}^{4+}(\text{UO}_2)\text{O}_4(\text{OH})_6(\text{H}_2\text{O})_9$ ($2\theta=11.64^\circ$) are candidates. It would be very difficult to identify the exact phase that is responsible for the 12.0° peak since the secondary diffraction peaks of the uranyl minerals coincides with the broad UO_2 peaks in this sample making confirmatory identification impossible. However, uranyl species are present. This result may appear to be somewhat surprising since one might expect an anoxic environment to produce UO_{2+x} but Haschke reported similar results [HASCHKE-1998] based on XRD where a mixture of UO_2 and hydrated UO_3 was detected under anoxic corrosion. Also, there is a small systematic shift in the UO_2 peak locations to higher 2θ that translates to a lower unit cell parameter indicative of excess oxygen above stoichiometry. This shift is expected based on Colmenares' review [COLMENARES-1984] on the occurrence of UO_{2+x} from the wet oxidation of uranium metal in the absence of oxygen. Quantitative evidence for hyperstoichiometric UO_{2+x} is provided by cell refinement which indicated UO_{2+x} with a calculated cell parameter⁵ of $5.445 \pm 0.007 \text{ \AA}$ compared to a value of 5.440 \AA for U_4O_9 ($\text{UO}_{2.25}$) and 5.468 \AA for $\text{UO}_{2.03}$ suggesting the spalled product is closer to $\text{UO}_{2.25}$ than $\text{UO}_{2.0}$. This finding is consistent with the presence of the uranyl compounds in the diffraction pattern and appears to agree with Haschke [HASCHKE-1998]. At the same time it differs from the results of Baker [BAKER-1966] who found the product oxide to be $\text{UO}_{2.06\pm 0.02}$ when oxygen was absent in the reaction. When the product oxide was subsequently exposed to oxygen at elevated temperatures the oxide $\text{UO}_{2.2\pm 0.1}$ was produced [BAKER-1966]. Due to the

⁵The cell parameter is a linear function of the oxygen content of the unit cell where hyperstoichiometry leads to a decreased cell parameter and hypostoichiometry leads to an increased cell parameter.

conflicting evidence presented here, by Haschke [HASCHKE-1998], and by Baker [BAKER-1966], it is difficult to determine whether the hyperstoichiometric UO_2 produced in this study is accurately characterized or a product of further oxidation during the analysis period. No uranium hydrides were detected.

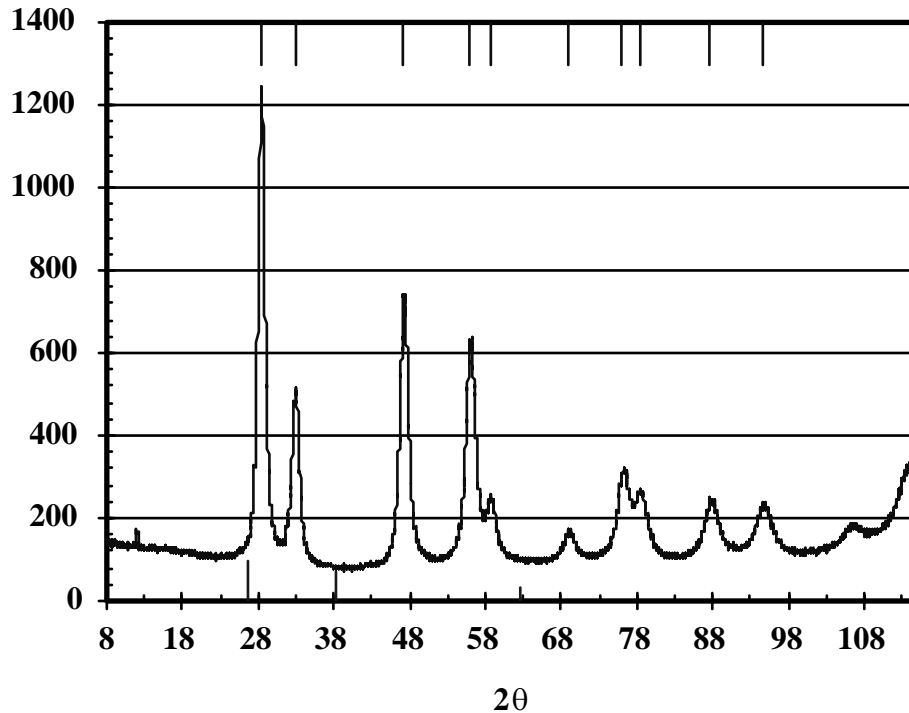


Fig. 9. X-ray Diffraction Pattern for Oxidized Uranium Metal in EJ-13 at 90°C (the Markings at the Top of the Plot Show Expected Peak Positions for Uraninite and Those at the Bottom Show Expected Peak Positions for UH_3 , Ruling Out the Presence of Hydrides in Levels Sufficient for XRD Detection)

Included in the cell refinement is an estimate of the diffracting domain size based on the full width at half-maximum of the peaks. The domain size for this material is <10 nm, which does not necessarily mean that individual particle sizes are 10 nm. But when one considers the TEM analysis of uranium colloids (see Section III.B.3) it is quite clear that uranium colloids are being generated as spheres with particle sizes of 5-10 nm. The TEM and XRD data then suggest that colloids are released into solution as a result of cleavage along crystal domains that form during the oxidation of the metal. Importantly then, the release of UO_{2+x} colloids occurs regardless of the presence of dissolved oxygen. If dissolved oxygen were a major participant, one would expect UO_3 -type colloids formed via dissolution and precipitation of dissolved uranyl species to dominate the colloid population. This conclusion is consistent with observations on the oxic and anoxic corrosion of uranium metal and occurrence of similar UO_{2+x} colloids in unreported, oxic drip tests run at ANL.

2. Gas Generation

As with UUBT1, the gas pressure was monitored (see Fig. 10). Pressurization could not be detected before day 6 because of a leaky gasket. Once again, there appears to be an induction period before the evolution of hydrogen defines the dominant corrosion mechanism. Compared to UUBT1 the oxygen levels in solution are extremely low, so it appears that the induction period is not a sensitive function of the O_2 concentration in solution. That is to say, the presence of 1/10 the oxygen levels in ambient air (Test UUBT1) displayed an induction period identical, to within experimental error, to that observed in Test UUBT2 where <50 ppm O_2 was present. The pressure in the vessel begins to increase 10-14 days into the test. The linear period between days 14 and 54 was used to estimate an oxidation rate of 0.94 mg/d based on a least squares fit of the data and corresponds to an estimated corrosion of 39 mg of fuel (46% of original fuel) during this period. If this value is normalized to the original fuel geometric surface area (assume same surface area as UUBT1, 23.2 mm^2), a highly conservative corrosion rate of $4 \times 10^5 \text{ mg/m}^2/\text{d}$ is obtained. No net production of gas was measured after day 55. A faulty gasket may have caused the failure to observe additional gas generation.

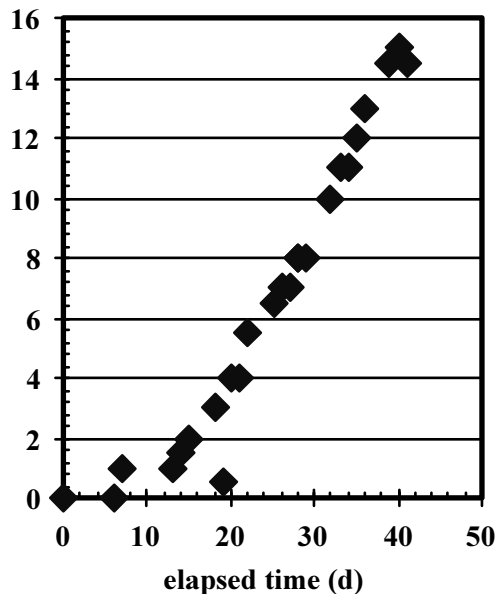


Fig. 10. The Inferred H_2 Gas Produced during the Corrosion of 84.1 mg of Uranium Metal in Test UUBT2

3. Colloids

The reacted solution was not analyzed for colloids until day 28, at which time the colloid population was detectable by DLS. It subsequently increased to exceptionally

high levels, indicated by extremely large scattering intensities for days 55 samples (1100×10^3 cps) and day 108 samples (1790×10^3 cps) as displayed in Table 6. When the light scattering software could generate acceptable data fits, a wide distribution was computed. The polydispersity indices were reasonably low to have confidence in the distribution histograms for some measurements but could not be reproduced with certainty. Typical size distribution outputs were $300 \text{ nm} \pm 300 \text{ nm}$ at FWHM. Of note is the scattering signal from the experimental blank UUBB1 after day 116. The strong scattering intensity suggests that EJ-13 itself is susceptible to colloid production under anoxic conditions. The TEM analysis of filtrate revealed the presence of smectite clays. In addition, the TEM data that follows will show that components of EJ-13 are probably contributing significantly to the colloid population.

The dissolved uranium concentration at the initial sampling (360 ppb) was similar to that in days 6 and 17 of UUBT1 (colloids were not filtered until day 55). By day 55 uranium colloids were prevalent. As seen in Fig. 11, colloidal uranium accounted for nearly all the detectable uranium at 55 days and approximately half of the uranium in solution at day 108. It is noted that nickel was found in solution well in excess of its EJ-13 concentrations and was partitioned to the colloidal range suggesting that the stainless steel vessel may be contributing to the nature of some colloidal species. No other metals (e.g., Si, Ca, Fe, Al) were found to be strongly partitioned to the colloidal phases based on solution analyses.

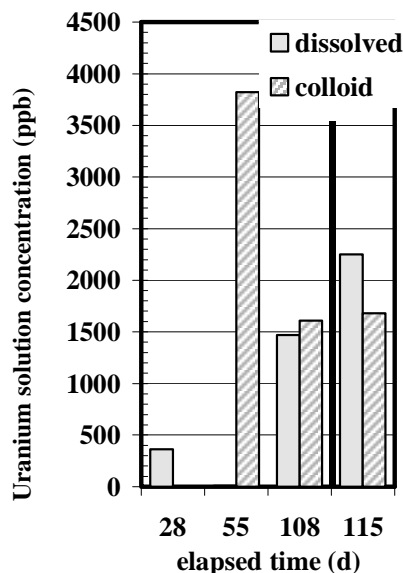


Fig. 11. Dissolved and Colloidal Uranium Concentrations in Solutions from Test UUBT2. (The vertical line indicates that the test was equilibrated with air after the sampling at 108 days.)

Table 6. Measured Light Scattering Intensity for Samples Withdrawn during Test UUBT2 (Laser Power = 3 mW)

Sample ^a	Oxic Level (anoxic or oxic)	Date of Analysis	No. of Days in Storage ^b	Poly- dispersity Index	Mean Particle Size	Light Scattering Intensity (x10 ³ cps) ^c	Calculated Particle Concentration ^d	Colloidal U Conc. (ng/mL) ^e	Dissolved U Conc. (ng/mL) ^f
day 28	Anoxic	2-28-01	6	0.32	310±260	160	2x10 ¹¹ (1x10 ¹⁰)	did not measure	361
⇒day 28	Anoxic	3-20-01	26	>0.5	could not resolve	4.5	8x10 ⁹ (3x10 ⁸)		
⇒day 28	Anoxic	6-26-01	124	0.36	(cnr) cnr	160	2x10 ¹¹ (1x10 ¹⁰)		
day 55	Anoxic	3-20-01	0	0.08	220±220	1100 (100 @ 150 µm PMT)	2x10 ¹² (7x10 ¹⁰)	3822	8
⇒day 55	Anoxic	4-3-01	14	0.18	190±170	100 @ 150 µm PMT			
⇒day 55	Anoxic	4-4-01	15	0.16	212±170	100 @ 150 µm PMT			
⇒day 55	Anoxic	6-26-01	98	0.6	cnr	170	2x10 ¹¹ (1x10 ¹⁰)		
day 108	Anoxic	5-15-01	5	0.4	cnr	1790 (90 @ 150 µm)	3x10 ¹² (1x10 ¹¹)	1610	1470
⇒day 108	Anoxic	6-12-01	33	0.5	cnr	253	5x10 ¹¹ (2x10 ¹⁰)		
⇒day 108	Anoxic	6-26-01	47	>0.6	cnr	230	4x10 ¹¹ (2x10 ¹⁰)		
day 115	Oxic	6-12-01	0	>0.5	cnr	552 (500 µm PMT) or 50 (150 µm PMT)	1x10 ¹² (4x10 ¹⁰)	1680	2250
Blank, UUBB1, day 116	Anoxic	6-26-01		>0.5	cnr	160	2x10 ¹¹ (1x10 ¹⁰)		

^a ⇒ indicates sample reanalyzed after storage

^b Number of days stored in <50 ppm O₂ at room temperature after removal from test vessel.

^c The scattered light passed through a 500-µm collimator unless a 150-µm collimator is specified.

^d Particle concentration estimated by assuming sample scattering intensity is identical to that of latex spheres of 100 nm diameter (300 nm diameter).

^e Uranium concentration associated with fraction of sample that passed through a 0.45 µm filter but not through a 30-kDa filter.

^f Uranium concentration with fraction of sample that passed through a 30-kDa filter.

The unfiltered solution at day 55 was wicked through a holey carbon grid and analyzed by TEM. This analysis offers a more accurate method of determining the disposition of elements within colloids. The results are displayed in Fig. 12. Colloids appeared to be composed of UO_2 spheres and smectite-type silicate clays. The uranium oxides existed as large agglomerates of tiny spheres <10 nm in diameter (Fig. 12a) or attached to silicate clay host materials. The uranium agglomerations varied in size from <50 μm to >200 μm . The morphology of the smectite clays (Fig. 12b) resembles that of layered clays found in waste glass corrosion [MERTZ-1999], with variations in size and shape. Not surprisingly, because of the nature of clays, Fe, Ni, and Al were found in association to varying degrees. The source of Fe may be either the EJ-13 or the vessel and the source of Ni must be the corrosion of the vessel. This diversity of both the UO_2 and silicate clay colloid morphology corroborates DLS measurements where size distribution data were difficult to reproduce due to large sample polydispersity.

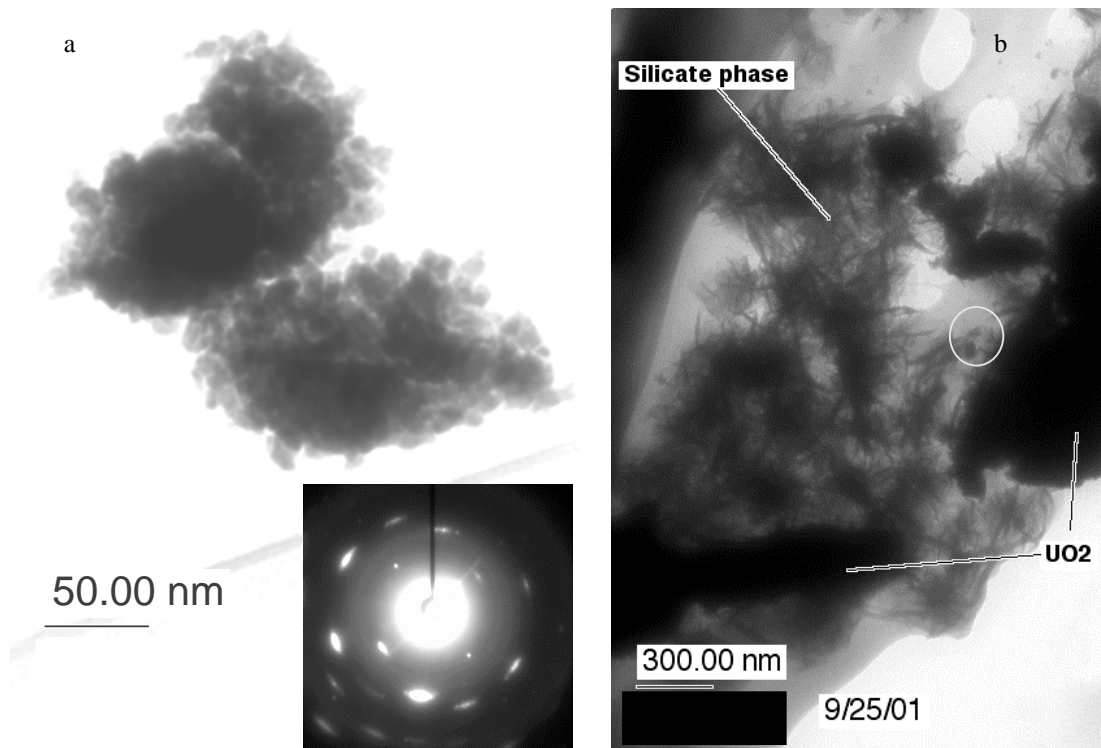


Fig. 12. TEM Images of Two Types of Colloids Found during Test UUBT2 Reveals (a) an Agglomeration of UO_2 Spheres and Electron Diffraction Pattern of Similar Structure and (b) the Rippled Morphology Typical of a Layered Smectite Clay Structure. Note the UO_2 spheres entrained in the clay (circled).

The stability of colloids was investigated as before and is shown in Table 6. Colloids collected at day 28 persisted in the sample after four months or storage

with scattering intensity equal to the initial evaluation (2-28-01), while the colloid signal was reduced from 1100×10^3 cps to 170×10^3 cps in the day 55 sample after three months storage. A similar decrease in signal intensity was observed after a one-month storage of the day 108 sample. The data suggest that uranium metal corrosion will produce copious amounts of colloids, which are at least partly unstable and will reduce in number with time. Still unknown is whether this instability is generated by changes in pH, temperature, vessel material, or by the absence of a precipitated source material (i.e., the uranium oxide products controlled by the solubility index). Also, it is still to be determined whether the decrease in colloid signal is due to disappearance of either UO_2 and clay or both.

This collection of data marked the termination of the anoxic tests. Test UUBT2 was restarted by exposing the vessel contents to normal air (21% O_2) and monitoring the effect on dissolved uranium and colloids. The next section summarizes the results of this short experiment.

C. Oxic Testing

After exposing the test UUBT2 to laboratory air for about 12 hours, the vessel was resealed and heated to 90°C as before. A sample was withdrawn at day 7 (115 days after UUBT2 initiation) and analyzed as previously described. The brown appearance of the spalled products was not visibly altered (e.g., no change in color) and the presence of colloids remained strong although the signal intensity did drop significantly, >1000 to 552 kcps (see Table 6). Uranium associated with the colloids was determined by filtration and was comparable to day 108, although the dissolved uranium concentration was 50% higher (see Fig. 11). There were no other significant differences between solution and colloidal elemental concentrations in the anoxic and oxic tests (see Table A4, Appendix A). Analysis of the colloids by TEM produced similar results as seen at 55 days, although calcium-rich colloids now were observed (see Fig. 13), in addition to UO_2 and clay colloids. The clays incorporated Al, Ni, Fe, and Mg.

There appear to be at least two mechanisms governing the corrosion of metallic uranium fuel in well water at 90°C . The first mechanism appears to dominate the initial corrosion while the fuel is relatively intact. No gas pressurization occurs during this induction period. The second mechanism produces a net gas release, presumed to be H_2 , as the fuel is completely converted to a fine UO_2 powder.

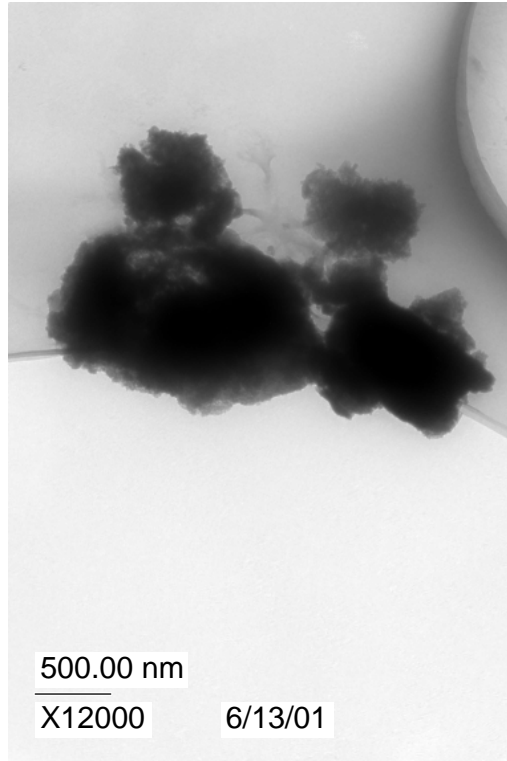


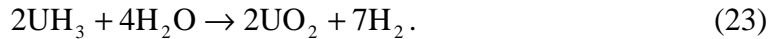
Fig. 13. Transmission Electron Micrographs of Calcium-Rich Colloids Collected at Day 115 under Oxidic Conditions in Test UUBT2. No other elements were detected by X-ray analysis of this colloid (oxygen could not be determined).

IV. DISCUSSION

The induction periods were 6 weeks and 1-2 weeks for test UUBT1 (2% O₂ in N₂) and UUBT2 (<100 ppm O₂ in N₂), respectively. If the induction period were a direct function of oxygen available in the test vessel, no induction period would have been expected to occur in UUBT2. Based on oxygen availability one can compute the fraction, f , of uranium that can be oxidized according to Eq. 3. For UUBT1, assume that the vessel was in equilibrium with the glovebox air ($C_{O_2} = 0.2$ mol fraction) at each sampling (five samplings), and that all the O₂ (dissolved and in vessel head-space) is available for reaction. The dissolved component turns out to be insignificant compared to the O₂ available in the headspace of the vessel. Using this approach the following fraction can be computed:

$$\frac{\left(C_{O_2} \frac{V_{head}}{22.4 \times 10^3} \right) / 2}{\left(m_U \frac{1}{238 \times 10^3} \right)} \times 100 \times n = f_{U \rightarrow UO_2} = 6\% \quad (22)$$

where V_{head} is the headspace volume in the vessel (7-11 mL), 22.4×10^3 is the conversion factor for moles of air per mL, $1/2$ is the stoichiometric ratio from Eq. 3 where $x=0$, m_U is the mass of uranium metal in mg, 238×10^3 is the conversion factor for moles of U per mg of fuel, and n is the number of times the vessel was sampled. Thus, the total oxygen available to the fuel can roughly account for 6% of the oxidized fuel, at which time H_2 production under Eq. 6 should dominate. And yet, the pressurization calculations show that H_2 can account for only <50% of the oxidized fuel. Using this exercise for test UUBT2, where the O_2 levels were >1000 times lower than in UUBT1, it is quite obvious that oxygen should not be a factor in the corrosion of the fuel. The results suggest that the corrosion of uranium under saturated anoxic conditions does not follow Eq. 2 exclusively. There must be additional mechanisms to account for the reduced H_2 production and the induction period corrosion. One such mechanism is removal of H_2 during the formation of uranium hydrides via Eq. 19, which would produce an accumulation of UH_3 that would subsequently release hydrogen by reaction with water:



Baker et al. [BAKER-1966] showed that UH_3 formation increased as the relative humidity and temperature increased producing up to 13% hydride under flowing gas conditions. The static conditions of this test may contribute to hydride concentrations higher than 13%. The similarities in density between hydride (10.95 g/cm^3) and oxide ($11-11.3 \text{ g/cm}^3$) suggest that both products could grow intimately without developing sufficiently large stresses. The lack of hydride in the diffraction analysis reduces the credibility of this argument although hydrides may have reacted with water to produce UO_2 before analysis could be completed. Reasons for the observed induction period needs further investigation.

Of prominent importance, colloids were generated in copious quantities compared to corrosion of other fuel types such as MOX [MERTZ-2001a], UAl_x [KAMINSKI-2001], and UO_2 [MERTZ-2001b]. These colloids are composed of isolated (<10 nm) or agglomerated uranium dioxide spheres and smectite clays. The agglomerated spheres and clay material displayed a variety of sizes from <50 nm to >500 nm. Light scattering measurements confirmed the polydispersity of the colloids and high colloid populations. Using the scattering intensities, colloid densities as high as 10^{12} particles/L were estimated. Uranium was associated with the colloid fraction in substantial concentrations: as much as 98.2% of the uranium released into solution (Test UUBT2, day 55). In this sample, the colloidal uranium concentration was 1.6×10^{-5} M, as opposed to a dissolved concentration of 3×10^{-8} M. The UO_{2+x} colloid spheres appear to form via cleavage along crystal domains 5-10 nm in size that are produced during the direct oxidation of the material as shown by X-ray diffraction. This is an important finding because it suggests that colloidal UO_2 is released directly during oxidation and is not

limited to the kinetics of oxidation, dissolution, and precipitation of uranyl-type colloids. The colloids produced in the fuel tests are at least partially stable for the durations monitored under this short program.

V. FUTURE WORK

The next phase in the testing of uranium metal fuel encompasses identical testing methodology for irradiated N-Reactor fuels. These tests have begun and will continue through the end of FY2001. Gas samples will be collected and analyzed as well to confirm the generation of H₂ gas. As part of the irradiated fuel testing program, the colloid samples collected under the unirradiated program discussed in this report will continue to be monitored for stability and paragenesis, as will colloid fractions generated by the fully irradiated fuels. The stability of colloids will be explored as to the effects from pH change and dilution. Finally, the colloids generated during the blank test UUBB1 will be examined further as to characterization and stability.

VI. ACKNOWLEDGMENTS

Modifications to the glovebox and Parr vessels were completed by J. Emery and M. Clark. The water analysis performed by S. Wolf and Y. Tsai was much appreciated. Also, thanks to J. Holly and J. Fortner for TEM and electron diffraction analysis, B. Finch for XRD analysis, and C. Mertz for sample preparation and assistance with DLS experiments. This work was supported by the U.S. Department of Energy, under contract W-31-109-ENG-38.

VII. REFERENCES

[BAKER-1966]

M. McD. Baker, L. N. Less, and S. Orman, *Trans. Faraday Soc.*, 62, 2513, 1966.

[COLMENARES-1984]

C. A. Colmenares, *Prog. Solid State Chem.*, 15, 257-364, 1984.

[MERTZ-2001a]

C. J. Mertz, personal communication with C. Mertz on the laser light scattering intensity for filtrate from MOX drip test at ANL, July 2001.

[MERTZ-2001b]

C. J. Mertz, personal communication with C. Mertz on the laser light scattering intensity for filtrate from commercial UO₂ fuel drip test at ANL, July 2001.

[FORTNER-2001]

J. A. Fortner, C. J. Mertz, M. M. Goldberg, and C. V. Shelton-Davis, "Corrosive Alteration of N-Reactor Fuel Exposed to Simulated Groundwater," *Proceedings of the 9th International High-Level Radioactive Waste Management Conference*, Las Vegas, NV, April 29-May 3, 2001.

[HASCHKE-1998]

J. M. Haschke, *J. Alloys Comp.*, 278, 149-160, 1998.

[KAMINSKI-2001]

M. D. Kaminski and M. M. Goldberg, "Corrosion of Breached Aluminide Fuels Under Potential Repository Conditions," *Proceedings of the 9th International High-Level Radioactive Waste Management Conference*, Las Vegas, NV, April 29-May 3, 2001.

[MCGILLIVRAY-1994]

G. W. McGillivray, D. A. Geeson, and R. C. Greenwood, *J. Nucl. Mat.*, 208, 81-97, 1994.

[MERTZ-1999]

C. Mertz, "Colloid-Associated Radionuclide Concentration Limits," *Office of Civilian Radioactive Waste Management Analysis Model Report*, ANL-EBS-MD-000020 REV 00 ICN 01, June 20, 1999.

[ORMAN-1964]

S. Orman, *Uranium, Compatibility Studies, Part 2: The Effect of Water Vapour Pressure in an Oxygen Free Atmosphere on the Corrosion Rate of Uranium at 100°C*, Atomic Weapons Research Establishment Report No. O-25/64, 1964.

[RITCHIE-1981]

A. G. Ritchie, *J. Nucl. Mater.*, 102, 170-182, 1981.

[WABER-1952]

J. T. Waber, Review of the Corrosion of Uranium and its Alloys, Los Alamos National Laboratory Report, LA-1524, 1952.

[WEIRICK-1984]

L. J. Weirick, The Oxidation of uranium in Low Partial Pressures of Oxygen and Water Vapor at 100 C, Report SAND-83-0618, Sandia National Laboratories, Albuquerque, NM, June 1984.

[WOLF-1998]

S. F. Wolf, J. Radioanal. Nucl. Chem., 235, 1-2, 207-212, 1998.

APPENDIX A

Raw Data and Measurement Tables

Table A1. Raw ICP-MS Data as Received from Analysis Report RFA#: I-010104-1. (Concentrations given in ng/g.) EJ-13A, B are stock solution samples from TSR#MK09. UUBT1d6-d refers to test UUBT1 collected at 6 days into the test and passed through a 30,000 MW filter (dissolved fraction). -c indicates a solution passed through a 0.45 μ m filter (colloid + dissolved fraction).

Element	Date of Analysis:		Analyst:		Submitted By:		M. Kaminski						Estimated Accuracy
	EJ-13A	EJ-13B	UUBT1d6-d	UUBT1d6-c	UUBT1d17-d	UUBT1d17-c	UUBT1d32-d	UUBT1d32-c					
Li	162	162	158	161	153	166	154	164					$\pm 10\%$
B	832	824	836	826	830	846	840	857					$\pm 10\%$
Na	5.54E+04	5.09E+04	5.65E+04	5.57E+04	5.25E+04	6.14E+04	5.70E+04	6.53E+04					$\pm 10\%$
Mg	117	148	116	36.2	83.5	83.4	101	107					$\pm 10\%$
Al	183	199	<17.6	<17.6	<17.6	<17.6	<17.6	<17.6					$\pm 10\%$
Si	3.98E+04	3.84E+04	3.48E+04	3.30E+04	2.86E+04	3.43E+04	2.65E+04	3.54E+04					$\pm 10\%$
P	439	456	571	595	453	477	460	486					$\pm 19\%$
K	1.27E+04	1.15E+04	1.28E+04	1.24E+04	1.20E+04	1.38E+04	1.27E+04	1.38E+04					$\pm 10\%$
Ca	8.69E+03	8.31E+03	7.30E+03	6.18E+03	6.22E+03	6.74E+03	4.93E+03	5.98E+03					$\pm 10\%$
Cr	<45.4	<45.4	<45.4	<45.4	<45.4	<45.4	<45.4	<45.4					$\pm 10\%$
Mn	<3.6	<3.6	14.3	13.2	49.3	29.7	<3.6	13.1					$\pm 10\%$
Fe	1.32E+03	1.32E+03	1.34E+03	1.49E+03	1.32E+03	1.52E+03	1.39E+03	1.55E+03					$\pm 10\%$
Zr	<0.7	<0.7	<0.7	<0.7	<0.7	<0.7	<0.7	<0.7					$\pm 10\%$
Au	<2.6	<2.6	<2.6	<2.6	<2.6	<2.6	<2.6	<2.6					$\pm 10\%$
U	<1.6	<1.6	512	499	518	427	2.66E+03	2.96E+03					$\pm 10\%$
^a Pu 239	<1.4	<1.4	<1.4	<1.4	<1.4	<1.4	<1.4	<1.4					$\pm 10\%$
^a Hg 202	3.31	2.83											$\pm 50\%$

^aSemi-quantitative.

Table A2. Raw ICP-MS Data as Received from Analysis Report RFA#: I-010327-3. (Concentrations given in ng/g, stock bottle TSR#MDK09 were sparged with N₂ gas and stored in the containment box. "EJ-D28" was sampled during the sampling of UUBT2 at day 28 on 2-22-01 and "EJ-13, 4-3-01" was sampled on 4-3-01.)

Element	EJ-D28	EJ-13, 4-3-01
Li	<8.3	<8.3
B	445	385
Na	4.12E+04	4.06E+04
Mg	276	256
Al	550	538
Si	3.20E+04	3.23E+04
P	358	438
K	8.82E+03	8.30E+03
Ca	7.58E+03	7.60E+03
Cr	2.43	2.4
Mn	2.1	1.91
Fe	<338	<338
Ni	17.7	4.38
Sr	37.7	36.3
Zr	1.07	1.73
Ru	<0.4	<0.4
Cs	1.57	1.56
Au	1.09	1.04
U	1.4	0.396
^a Tc 99	<0.1	<0.1
^a Np 237	<0.1	<0.1
^a Pu 239	<0.1	<0.1
^a Am 241	<0.1	<0.1
^a Cm 244	<0.1	<0.1
^a Cs137	0.242	0.482
^a Sr90	0.710	0.574

^aSemi-quantitative.

Table A3. Raw ICP-MS Data as Received from Analysis Report RFA#: I-010327-3.
(Concentrations given in ng/g). Sample ID Coded as in Table A1.

Date of analysis:	4/3/01			
Submitted by:	M. Kaminski		Analyst:	Y. Tsai
Dilution Factor	10	10	10	
Element	UUBT2d28-c	UUBT2d55-d	UUBT2d55-c	Estimated Accuracy
Li	<8.3	<8.3	<8.3	±10%
B	397	363	348	±10%
Na	4.86E+04	5.48E+04	4.26E+04	±10%
Mg	50.4	52.7	67.9	±10%
Al	145	124	195	±10%
Si	2.71E+04	1.48E+04	1.50E+04	±10%
K	1.01E+04	1.14E+04	1.28E+04	±10%
Ca	1.43E+03	1.19E+03	1.02E+03	±10%
Cr	4.79	5.16	6.67	±10%
Fe	<345	<345	<345	±10%
Ni	180	38.1	178	±10%
U	361	8.21	3.83E+03	±10%

Table A4. Raw ICP-MS Data as Received from Analysis Report RFA# I-010620-1. Sample ID Coded as in Table A1.

Element	Date of analysis: 6/21/01& 6/22/01										Accuracy	
	EJ1-6/17/01	EJ2-6/17/01	UUBB1d116-d	UUBB1d116-c	UUBT2d108-d	UUBT2d108-c	UUBT2d115-d	UUBT2d115-c	UUBT2d115-d	UUBT2d115-c		
Li	<39.5	<39.5	<39.5	<39.5	<39.5	<39.5	<39.5	<39.5	<39.5	<39.5	<39.5	±10%
B	1.09E+03	972	1.22E+03	1.07E+03	1.16E+03	1.17E+03	1.15E+03	1.15E+03	1.15E+03	1.15E+03	1.05E+03	±10%
Na	4.32E+04	4.19E+04	5.26E+04	5.08E+04	7.62E+04	8.05E+04	7.10E+04	7.10E+04	7.10E+04	7.10E+04	7.00E+04	±10%
Mg	366	422	323	305	427	212	245	245	245	245	172	±10%
Al	889	884	473	494	666	732	630	630	630	630	700	±10%
Si	3.66E+04	3.32E+04	3.71E+04	3.59E+04	2.64E+04	2.80E+04	2.72E+04	2.72E+04	2.72E+04	2.72E+04	2.58E+04	±10%
P	<297	<297	369	351	347	340	308	308	308	308	445	±10%
K	9.27E+03	8.92E+03	1.08E+04	9.76E+03	1.18E+04	1.18E+04	6.27E+03	6.27E+03	6.27E+03	6.27E+03	5.88E+03	±10%
Ca	9.25E+03	9.11E+03	1.09E+04	1.02E+04	2.61E+03	2.36E+03	2.86E+03	2.86E+03	2.86E+03	2.86E+03	2.51E+03	±10%
Cr	6.05	5.94	9.29	7.42	8.37	5.98	6.95	6.95	6.95	6.95	5.95	±10%
Mn	5.32	7.24	38.9	36.4	7.38	6.29	7.78	7.78	7.78	7.78	5.08	±10%
Fe	693	664	680	711	771	685	742	742	742	742	654	±10%
Ni	6.63	7.25	13.9	13	1.02E+03	83.6	27.1	27.1	27.1	27.1	34.9	±10%
Sr	41.8	38.5	49.2	42	<5.1	<5.1	<5.1	<5.1	<5.1	<5.1	<5.1	±10%
Zr	3.46	3.44	3.33	3.47	3.67	3.41	3.31	3.31	3.31	3.31	3.34	±10%
Ru	<0.2	<0.2	<0.2	<0.2	<0.2	<0.2	<0.2	<0.2	<0.2	<0.2	<0.2	±10%
Cs	2.25	1.81	2.25	2.09	1.86	1.81	1.25	1.25	1.25	1.25	1.16	±10%
Au	2.59	2.5	2.62	2.5	2.49	2.42	2.51	2.51	2.51	2.51	2.46	±10%
U	1.73	1.74	1.33	1.52	1.47E+03	3.08E+03	2.25E+03	2.25E+03	2.25E+03	2.25E+03	3.93E+03	±10%
^a Sr 90	0.114	0.118	<0.1	0.131	0.216	0.105	<0.1	<0.1	<0.1	<0.1	<0.1	±10%
^a Tc 99	<0.1	<0.1	<0.1	<0.1	<0.1	<0.1	<0.1	<0.1	<0.1	<0.1	<0.1	±10%
^a Cs 137	0.731	0.784	0.848	0.986	0.292	0.2	0.303	0.303	0.303	0.303	0.16	±10%
^a Np 237	<0.1	<0.1	<0.1	<0.1	<0.1	<0.1	<0.1	<0.1	<0.1	<0.1	<0.1	±10%
^a U 238	0.629	0.641	<0.3	0.416	1.55E+03	3.24E+03	2.36E+03	2.36E+03	2.36E+03	2.36E+03	4.14E+03	±10%
^a Pu 239	<0.2	<0.2	<0.2	<0.2	<0.2	<0.2	<0.2	<0.2	<0.2	<0.2	<0.2	±10%
^a Am 241	<0.1	<0.1	<0.1	<0.1	<0.1	<0.1	<0.1	<0.1	<0.1	<0.1	<0.1	±10%
^a Cm 244	<0.1	<0.1	<0.1	<0.1	<0.1	<0.1	<0.1	<0.1	<0.1	<0.1	<0.1	±10%

^aSemi-quantitative.

Table A5. Test Vessel Pressure Measurements Used to Estimate Uranium Oxidation Rates for Test UUBT1

Date	Reading (psig)	H ₂ Pressure (psig)	Elapsed # of Days	H ₂ Generated (moles)	Uranium Oxidized (g of metal)
6-Nov	11	0	0	0.0E+00	0.0E+00
14-Nov	16	5	8	1.2E-04	1.5E-02
16-Nov	18.5	7.5	10	1.8E-04	2.2E-02
20-Nov	22	11	14	2.7E-04	3.2E-02
22-Nov	23	12	16	3.0E-04	3.5E-02
27-Nov	25.25	14.25	21	3.5E-04	4.2E-02
28-Nov	25.1	14.1	22	3.5E-04	4.1E-02
11-Dec	25.25	14.25	35	3.5E-04	4.2E-02

Table A6. Test Vessel Pressure Measurements Used to Estimate Uranium Oxidation Rates for Test UUBT2

Date	Reading (psig)	H ₂ Pressure (psig)	Elapsed # of days	H ₂ Generated (moles)	Uranium Oxidized (g of metal)
25-Jan	0	0	0	0	0
31-Jan	8	0	6	0	0
1-Feb	9	1	7	1.6016E-05	0.0019059
7-Feb	9	1	13	1.6016E-05	0.0019059
8-Feb	9.5	1.5	14	2.4024E-05	0.00285885
9-Feb	10	2	15	3.2032E-05	0.0038118
12-Feb	11	3	18	4.8048E-05	0.00571769
13-Feb	8.5	0.5	19	8.008E-06	0.00095295
14-Feb	12	4	20	6.4064E-05	0.00762359
15-Feb	12	4	21	6.4064E-05	0.00762359
16-Feb	13.5	5.5	22	8.8088E-05	0.01048244
19-Feb	14.5	6.5	25	0.0001041	0.01238833
20-Feb	15	7	26	0.00011211	0.01334128
21-Feb	15	7	27	0.00011211	0.01334128
22-Feb	16	8	28	0.00012813	0.01524718
22-Feb	12	0	28	0, sampled	0
23-Feb	12	0	29	0	0
26-Feb	14	2	32	3.2032E-05	0.0038118
27-Feb	15	3	33	4.8048E-05	0.00571769
28-Feb	15	3	34	4.8048E-05	0.00571769
1-Mar	16	4	35	6.4064E-05	0.00762359
2-Mar	17	5	36	8.008E-05	0.00952949
5-Mar	18.5	6.5	39	0.0001041	0.01238833
6-Mar	19	7	40	0.00011211	0.01334128
7-Mar	18.5	6.5	41	0.0001041	0.01238833
20-Mar	23	11	54	0.00017618	0.02096487

Table A7. Analysis and Cell Parameters for X-ray Diffraction of Oxidized Uranium Metal from Test UUBT2 Day 108

USER: BFINCH	JADE: Cell Refinement Report	Anode=Cu						
FILE: UUBT2108.RAW	DATE: 06-30-01@05:19							
IDEN: anoxic slow scan								
SCAN: Range=8.0-115.0° in steps of 0.02°	Dwell time=12(sec)							
FIND: Filter=19p Threshold=3.0s	Cutoff=1.0% 2 θ =Centroid							
Cell Type = Cubic (F-Center)	Space Group = Fm3m (225)							
Refined Cell = 5.44481(0.00668)	Vol = 161.42 Å ³							
2 θ Error Window = 0.3	Zero Offset = 0.0471±0.1115°	ESD of Fit = 0.0939						
Least-Square Weighting>	Angular Weight = $\sqrt{(\text{Sin}\theta)}$	Angular Range = 8.0 - 115.0°						
h	k	l	2 θ c	2 θ o	2 θ c-o	dc	d _o	dc-o
1	1	1	28.415	28.447	-0.032	3.1385	3.135	0.0035
2	0	0	32.919	32.799	0.12	2.7186	2.7283	-0.0097
2	2	0	47.221	47.365	-0.144	1.9232	1.9177	0.0055
3	1	1	56.012	56.031	-0.018	1.6404	1.6399	0.0005
2	2	2	58.737	58.722	0.015	1.5706	1.571	-0.0004
4	0	0	68.974	69.011	-0.037	1.3604	1.3598	0.0006
3	3	1	76.192	76.114	0.078	1.2485	1.2496	-0.0011
4	2	0	78.543	78.411	0.132	1.2169	1.2186	-0.0017
4	2	2	87.793	87.926	-0.133	1.1109	1.1096	0.0013
5	1	1	94.679	94.665	0.014	1.0475	1.0476	-0.0001
4	4	0	106.36	-----	-----	0.9622	-----	-----
5	3	1	113.686	-----	-----	0.9201	-----	-----
			Avg.	$\Delta 2\theta = 0.072$		$\Delta d = 0.0024$		

APPENDIX B

TEM Reports

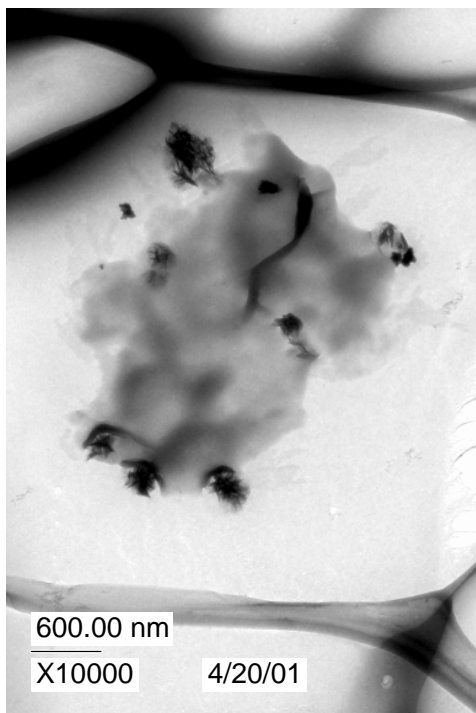
This section reproduces the TEM Analysis Reports supplied by J. Holly et al. for samples UUBT2 collected at 55, 108, and 115 days. No additional annotations were incorporated except those provided by J. Holly et al.

TEM Survey Report for Mike Kaminski
 April 24, 2001
 Microscopy Analyst: Jennifer Holly
 Sample ID: UUBT2D55
 Colloid sample # C423

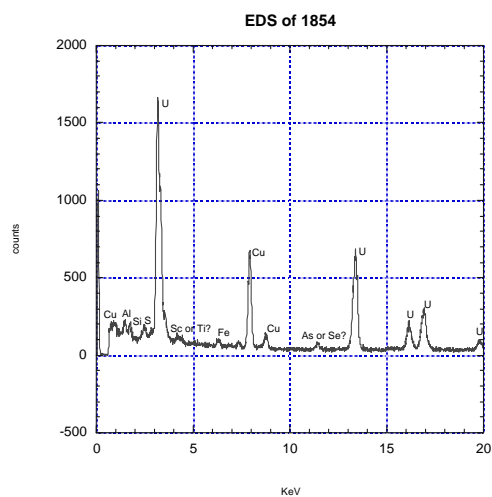
This sample was analyzed during the third week of April. There are nine images and nine EDS spectra in the pages that follow. The particles appear to be as small as 10 nm. They are clustered into masses ranging in size from 200 nm down to 50 nm. The images and spectra acquired are found in the pages that follow. All the copper peaks are artifacts due to the copper grid. A summary table lists the images and the EDS findings.

Sample ID: TEM Colloids Grid C423 from Sample UUBT2D55 for Mike Kaminski

Notebook Ref.	Digital Image Nos.	Comments and Elements identified by EDS
SN1718:79	1853	Low magnification overview of several particles. EDS was not performed.
SN1718:79	1854	Al, Si, S, Fe, Ti or Sc? As or Se and Uranium.
SN1718:79	1855	Large amounts of Si and Ni, Smaller amounts of Fe, Al, S, Cl, Ca, and Zn. There may also be Uranium present in a very small amount. The only peak visible for Uranium is at 3.171.
SN1718:79	1856	Al, Si, Cl, Ti or V? Fe, Se? and Uranium.
SN1718:78	1857	Al, Si, S, Cl, Ti or V?, Fe, Zn, Se?, and Uranium.
SN1718:80	1858	Al, Si, S, Cl, Ti or V?, Fe, Se?, and Uranium.
SN1718:80	1859	CCD 1859 is a low magnification overview of three particles. EDS 1859 is of particle 1 in CCD 1859. EDS spectrum identified Al, Si, S, Fe, Se?, and Uranium.
SN1718:80	1860	CCD 1860 is a high magnification image of particles 1 and 2 in CCD 1859. EDS 1860 is of particle 2. EDS spectrum identified Al, Si, S, Fe, Se?, and Uranium.
SN1718:80	1861	CCD 1861 is a high magnification image of particle 3 in CCD 1859. The EDS is also of particle 3. EDS spectrum identified Al, Si, S, Fe, Se?, and Uranium.



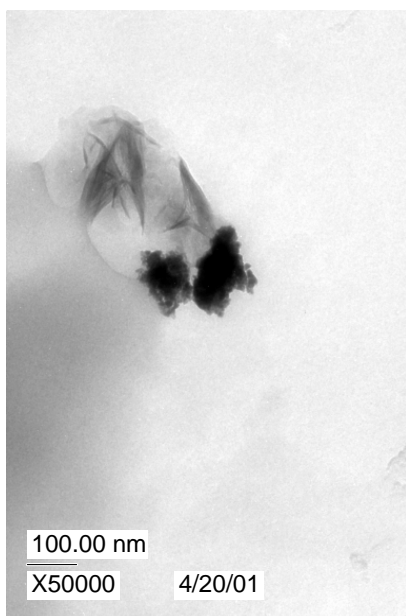
CCD 1853 - This is a low magnification overview of several particles. EDS was not performed. CCD images 1854-1857 are higher magnifications of particles in this image.



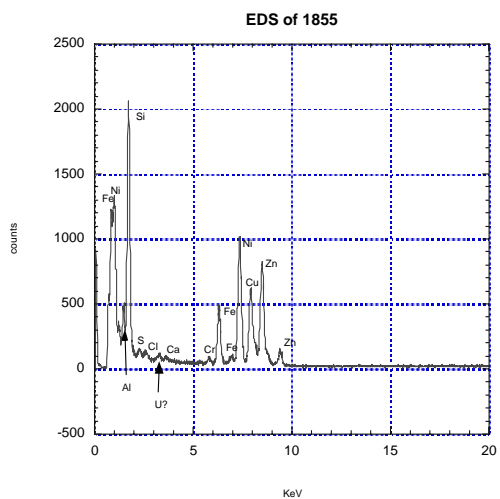
EDS of the Two Particles in CCD 1854



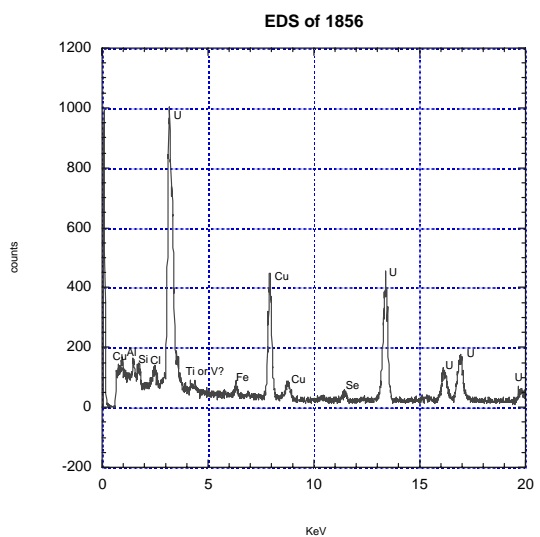
CCD 1855



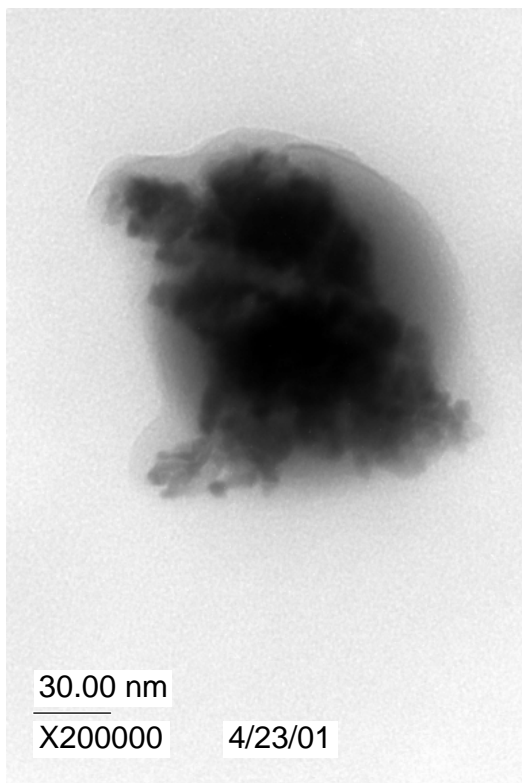
CCD 1854



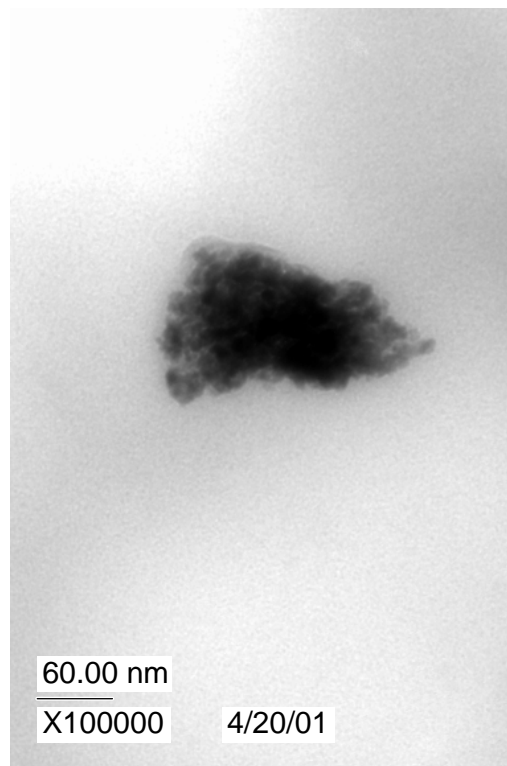
EDS of the Dark Area in CCD 1855



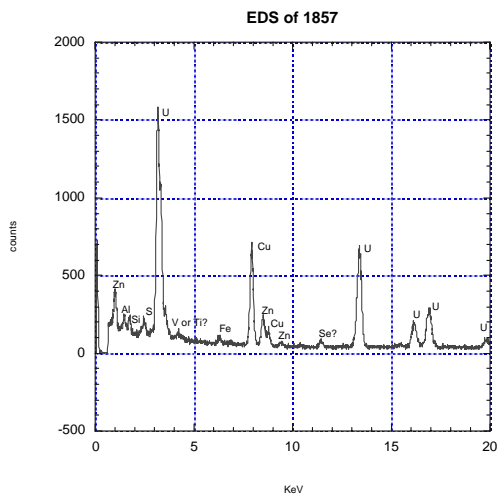
EDS of the Particle in CCD 1856



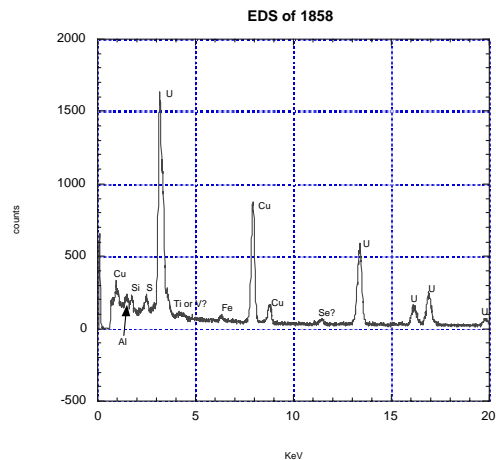
CCD 1856



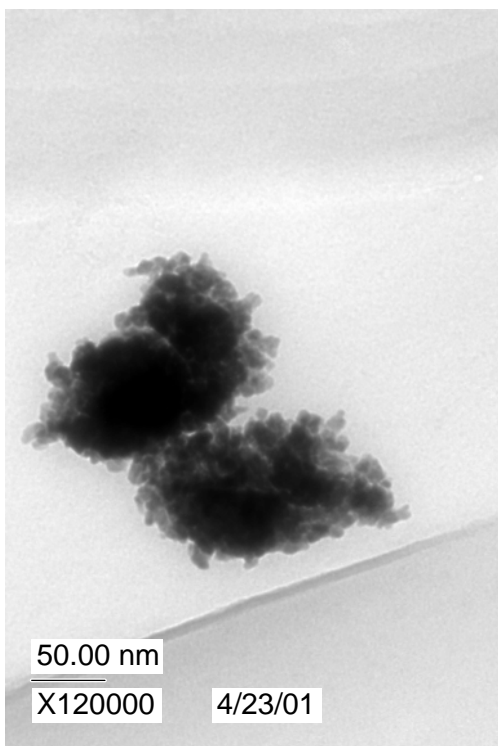
CCD 1857



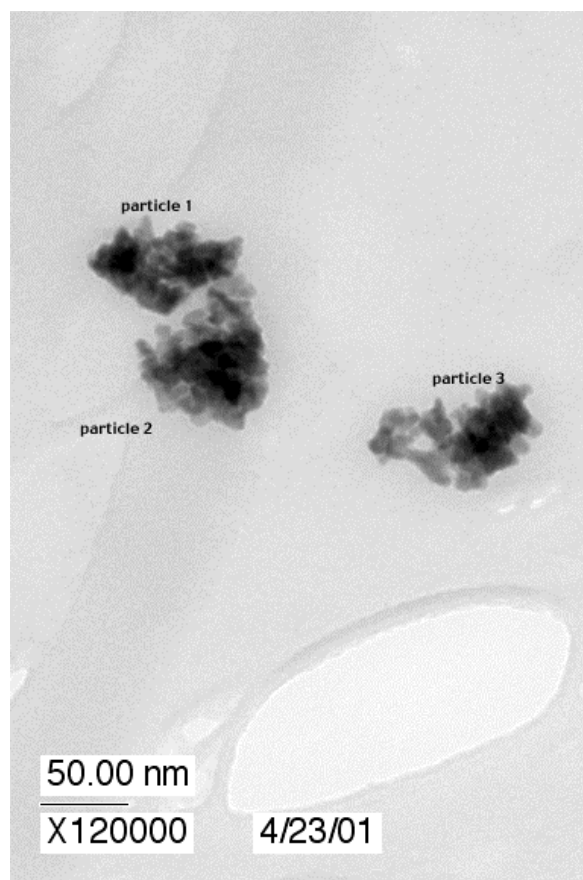
EDS of the Particle in CCD 1857



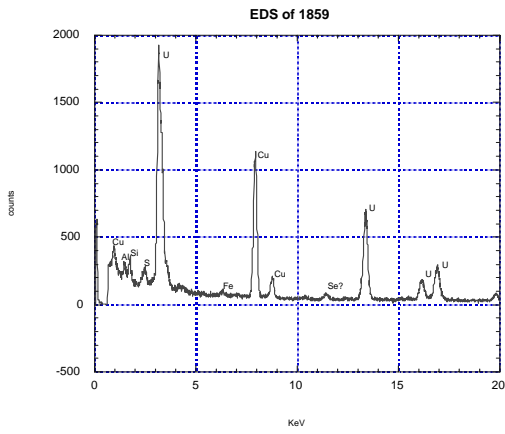
EDS of the Two Particles in CCD 1858



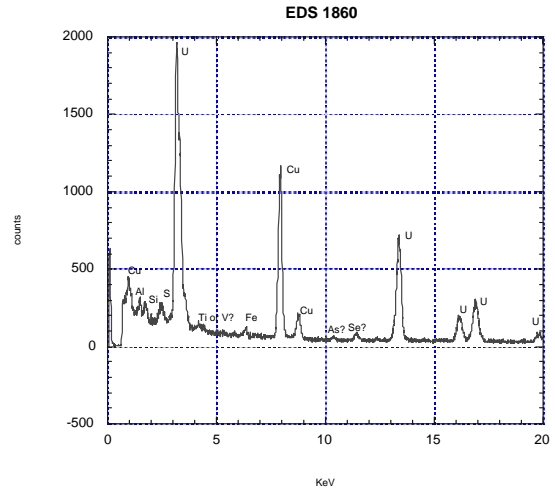
CCD 1858



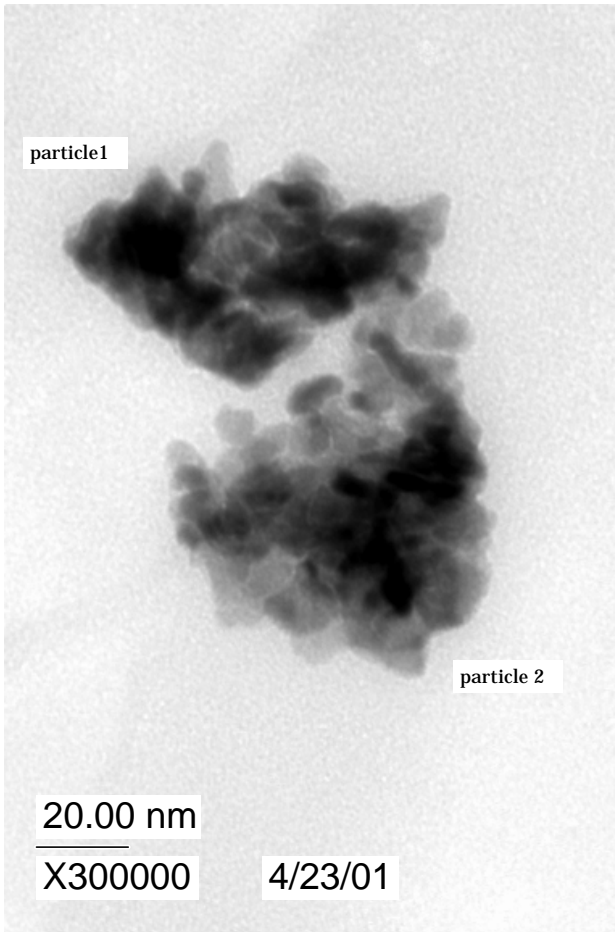
CCD 1859



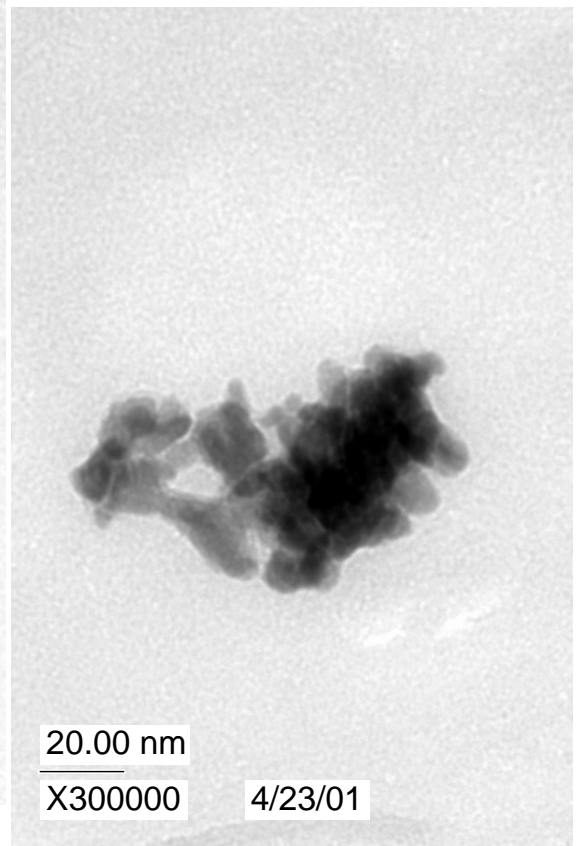
EDS of Particle 1 in CCD 1859



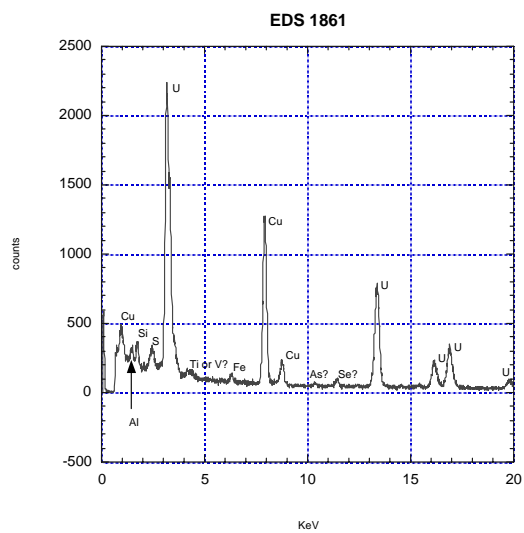
EDS of Particle 2 in CCD 1859 and in CCD 1860



CCD 1860 - This is a high magnification image of particles 1 and 2 from CCD 1859.



CCD 1861 - This image is of particle 3 in CCD 1859.



EDS of Particle 3 in CCD 1861 and 1859

TEM Survey Report for Mike Kaminski
 Microscopy Analyst: Jennifer Holly and Jeff Fortner
 Sample ID: UUBT2-D108

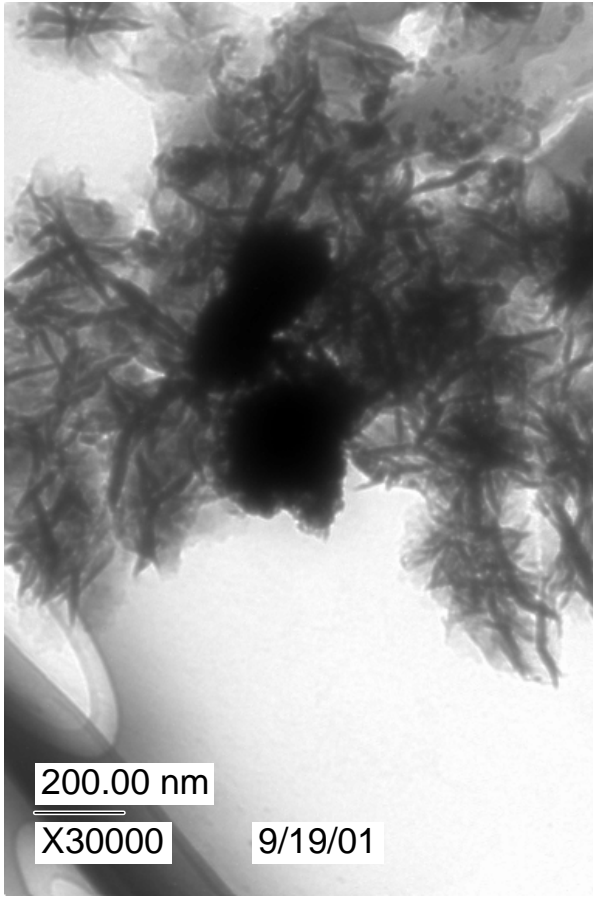
October 1, 2001

Colloid sample grid # C 448

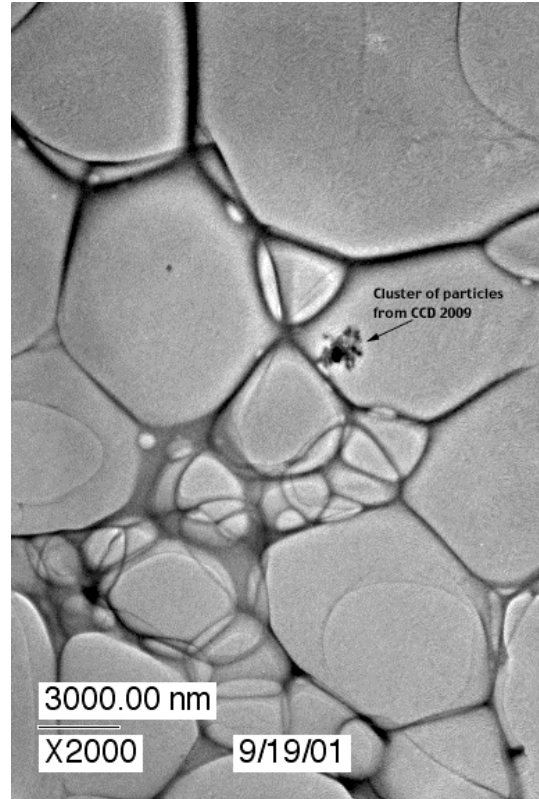
This sample was analyzed during the last two weeks of September. This sample is of colloids that have been wicked through a lacey carbon grid. There are 9 images, 1 diffraction pattern and 7 EDS spectra in the pages that follow. The images and spectra acquired are found in the pages that follow. All the copper peaks are artifacts due to the copper grid. A summary table lists the images and the EDS findings. The low magnification images were taken to show relative concentration of particles per grid square. A true analysis of concentration is nearly impossible using a TEM. An approximate analysis of concentration could be obtained with several days of TEM imaging and extrapolation, if necessary.

Table 1. Sample ID: TEM Colloids-Grid CC448, of Sample UUBT2-108 for Mike Kaminski

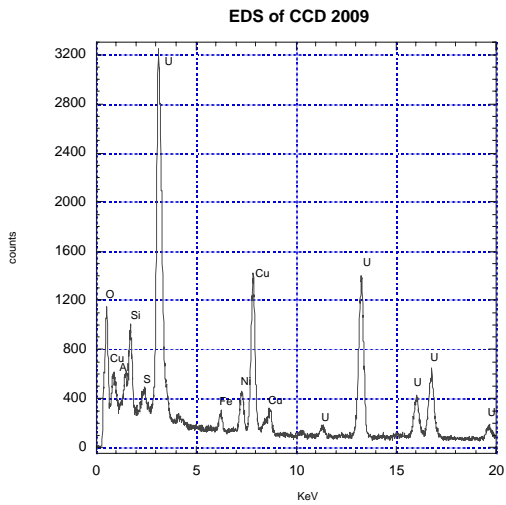
Block #	Grid #	Notebook Ref.	Digital Image or EDS File Numbers	Comments and Elements Identified by EDS
NA	C448	SN1718: 107	2009	Large amount of U and smaller amounts of Al, Si, S, Ni and Fe.
NA	C448	SN1718: 107	2010	NO EDS -This is a low magnification overview image.
NA	C448	SN1718: 107	2011	NO EDS-This is a low magnification overview image.
NA	C448	SN1718: 107	2012	Large amount of U and smaller amounts of Al, Si, S, Ni and Fe.
NA	C448	SN1718: 107	2013	NO EDS – This image is a low magnification overview.
NA	C448	SN1718: 107	2014	Large amount of Ti and smaller amounts of Si , Fe, and maybe Co.
NA	C448	SN1718: 107	2015	Large amount of U and smaller amounts of Al, Si, S, Ni and Fe
NA	C448	SN1718: 107	2016	Large amount of U and smaller amounts of Al, Si, S, Ni and Fe
NA	C448	SN1718:107& 108	2017	CCD image only. The two EDS form this image have been assigned different file numbers.
NA	C448	SN1718: 107	EDS 2018	EDS of the light material in CCD 2017
NA	C448	SN1718: 107	EDS 2019	EDS of the dark material in CCD 2017. Large amount of U and smaller amounts of Al, Si, S, Ni, Zn and Fe.
NA	C448	SN1718: 107	2020 diffraction composite	Diffraction of dark material in CCD 2017.



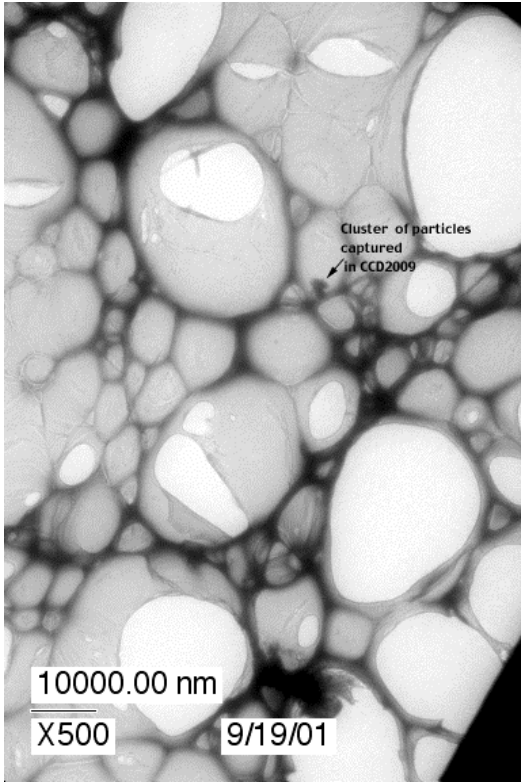
CCD 2009



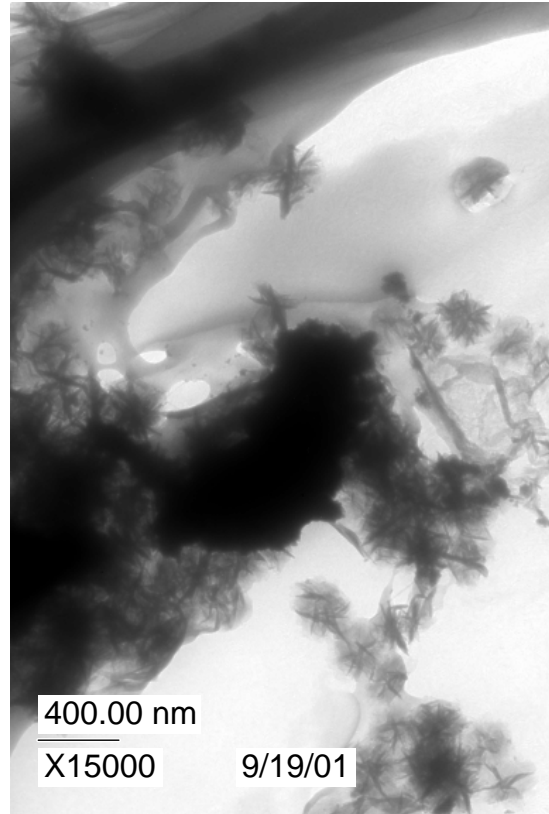
CCD 2010 - Low Magnification Overview of the Cluster of Particles in CCD 2009



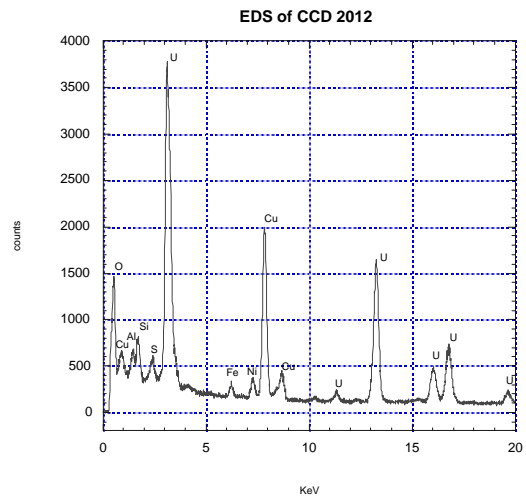
EDS of the Dark Particles in the Center of CCD 2009



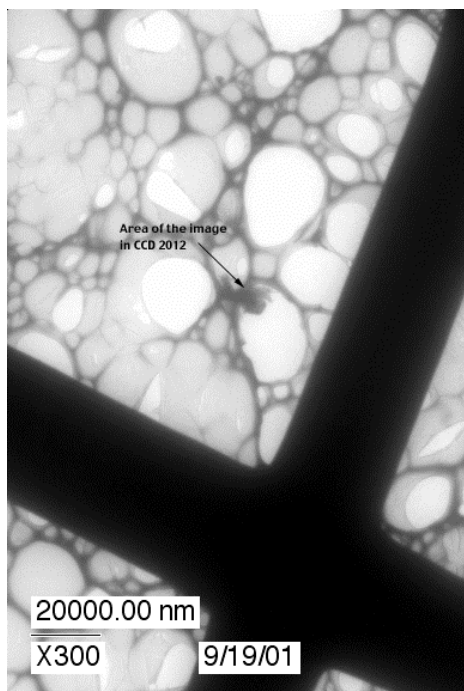
CCD 2011 - Lowest Possible Magnification Image Where the Particles Captured in CCD 2009 Still Remain Visible



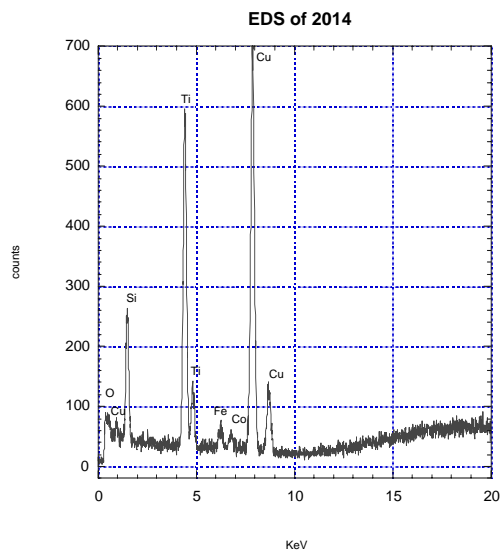
CCD 2012



EDS of the Dark Particle in the Center of CCD 2012



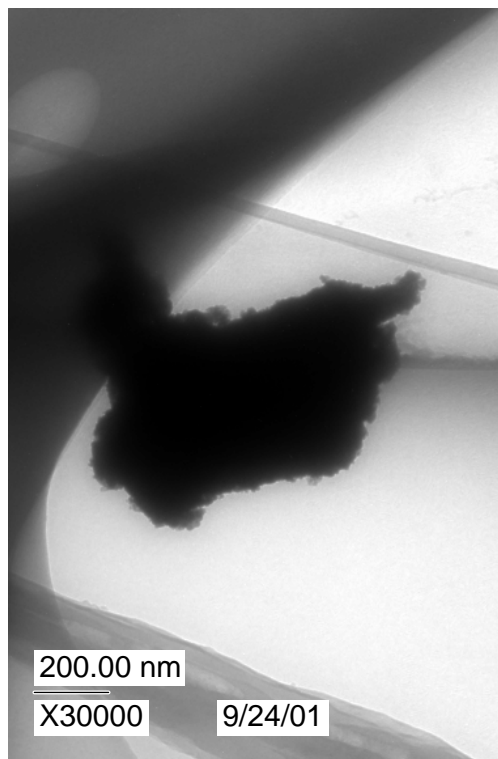
CCD 2013 - Low Magnification Overview of the Area Where CCD 2012 Was Captured



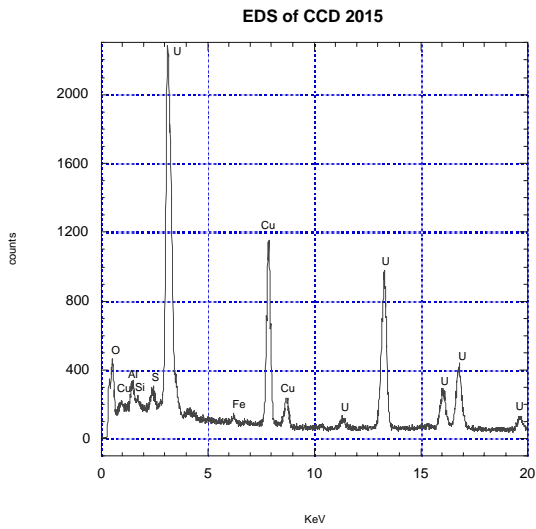
EDS of the Indicated Area in CCD 2014



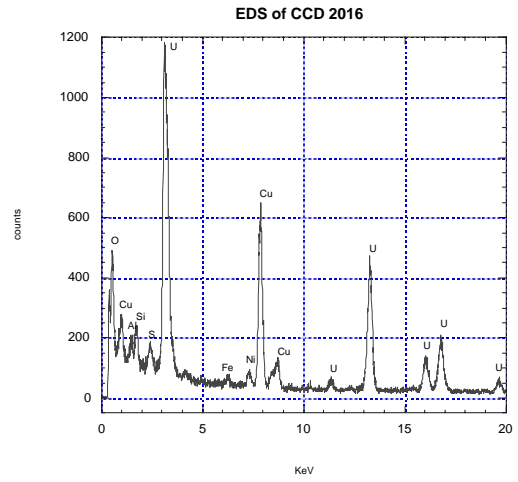
CCD 2014



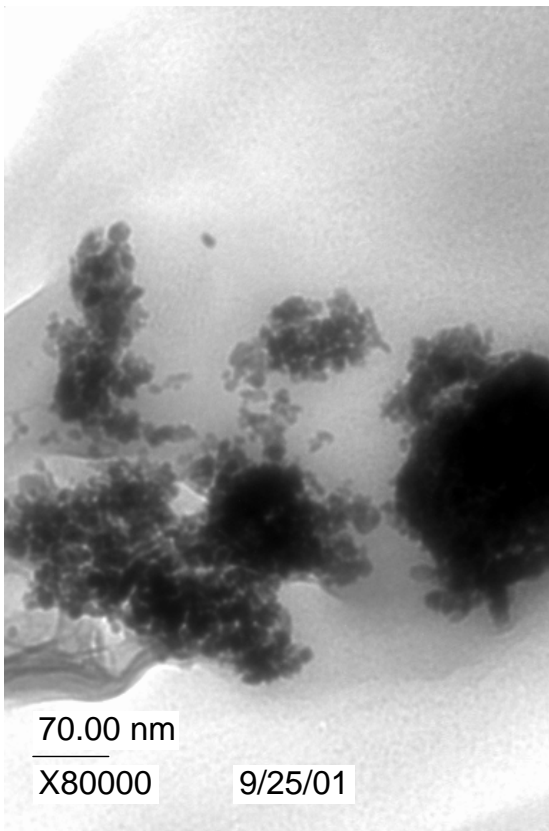
CCD 2015



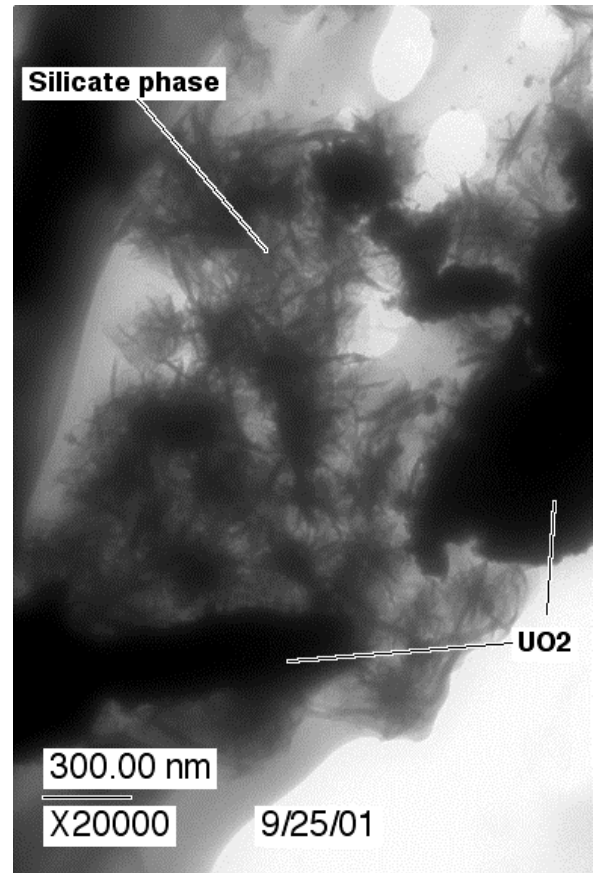
EDS of the Indicated Area in CCD 2015



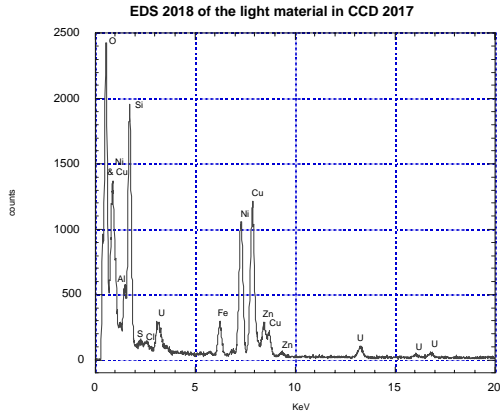
EDS of the Dark Particle in the Center of CCD 2016



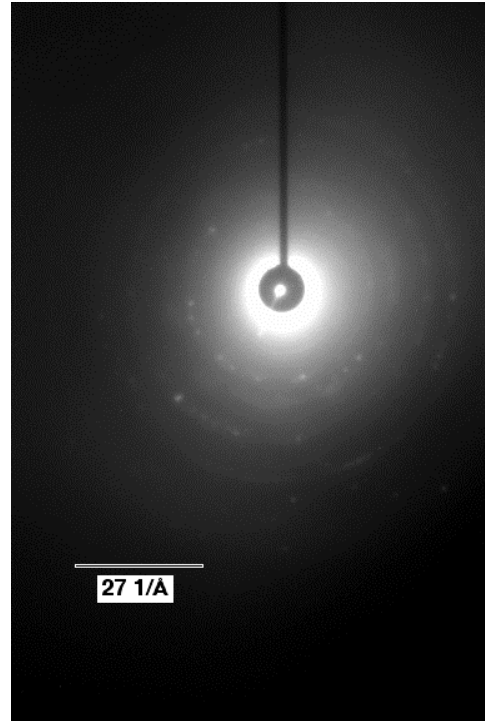
CCD 2016 - Unfortunately, this area became unstable in the beam and the carbon film ripped before I was able to obtain a diffraction pattern.



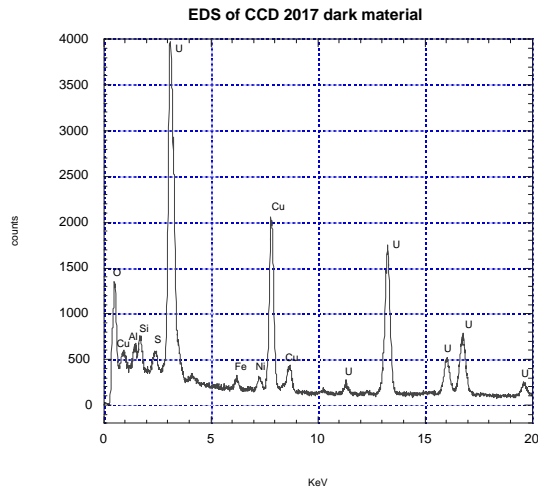
CCD 2017 - This image has two corresponding EDS spectra. EDS 2018 is of the UO₂ and EDS 2019 is of the silicate material. The diffraction pattern 2020 is of the dark material labeled as UO₂.



EDS of the Lighter Material (Labeled as Silicate) in CCD 2017



Diffraction 2020 - This composite diffraction pattern is from the dark material in CCD 2017 (labeled as UO_2) See diffraction analysis on the following page.



EDS of the Dark Material in CCD 2017 (Labeled as UO_2) in the Image

Diffraction Image 2020-Composite (R = 100 cm)^a

Pixels	Q (1/Å)	d-spacing (Å)	error (\pm Å)	UO ₂ (JCPDS-ICDD 78-0725)	UO _{1.96} (JCPDS-ICDD 75-0413)
49	1.328	4.732	± 0.09		
72	1.951	3.220	± 0.04	3.155	3.159
88	2.385	2.635	± 0.03	2.733	2.736
119	3.225	1.948	± 0.02	1.933	1.935
138	3.740	1.680	± 0.01	1.680	1.65
151	4.092	1.535	± 0.01	1.578	1.58

^a Likely sub-stoichiometric UO₂.

TEM Survey Report for Mike Kaminski
 Microscopy Analyst: Jennifer Holly
 Sample ID: UUBT2-D115

July 2, 2001

Colloid Sample Grid # C 433

This sample was analyzed during the second week of June. There are 9 images and 8 EDS spectra in the pages that follow. The particles appear to be as small as 5 nm. Some particles are clustered into masses ranging in size from 1500nm down to 90nm. The images and spectra acquired are found in the pages that follow. All the copper peaks are artifacts due to the copper grid. A summary table lists the images and the EDS findings.

Table 1. Sample ID: UUBT2-D115 for Mike Kaminski

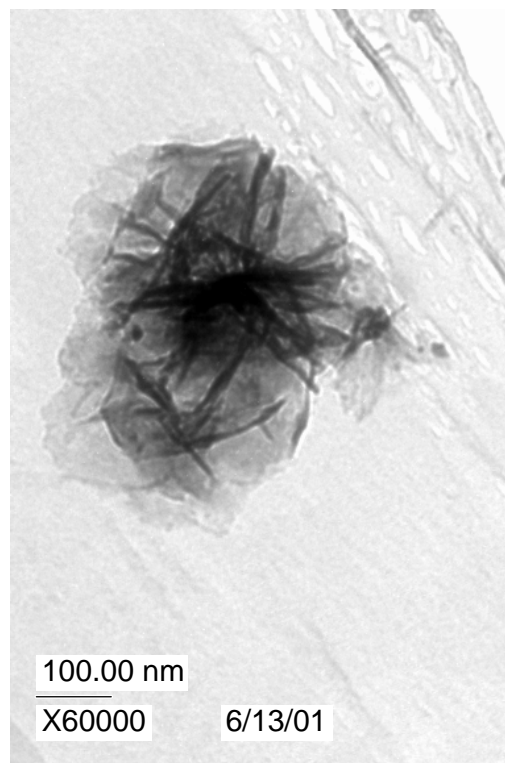
Block #	Grid #	Notebook Ref.	Digital Image Nos.	Comments and Elements Identified by EDS
NA	C433	SN1718:89	1930	Large amounts of Si, and Ni with smaller amount of Al, S, Cl, Ca, U, Fe, and Zn.
NA	C433	SN1718:89	1931	Large amounts of Si, and Ni with smaller amount of Al, S, Cl, Ca, U, Fe, and Zn.
NA	C433	SN1718:89	1932	Ca-rich material.
NA	C433	SN1718:89	1933	A low magnification overview image of the area in CCD 1934,1935, and 1936. No EDS was performed.
NA	C433	SN1718:89	1934	A high magnification image of the light round material in CCD 1933. EDS results: Large amount of Ca and smaller amount of Mg, Si, S and U.
NA	C433	SN1718:89	1935	Large amount of U and smaller amounts of Cl, Si, Al, and S.
NA	C433	SN1718:89	1936	Large amounts of Si, and Ni with smaller amount of Al, S, Cl, Ca, U, Fe, and Zn.
NA	C433	SN1718:90	1937	Large amount of U and smaller amounts of O, Si, Al, and S.
NA	C433	SN1718:90	1938	Large amount of U and smaller amounts of O, Si, Al, Fe, and S.
NA	C433	SN1718:90	1956	Large amount of U and smaller amounts of O, Si, and Al. Unfortunately, this particle was too thick for diffraction.

Table 1. Cont.

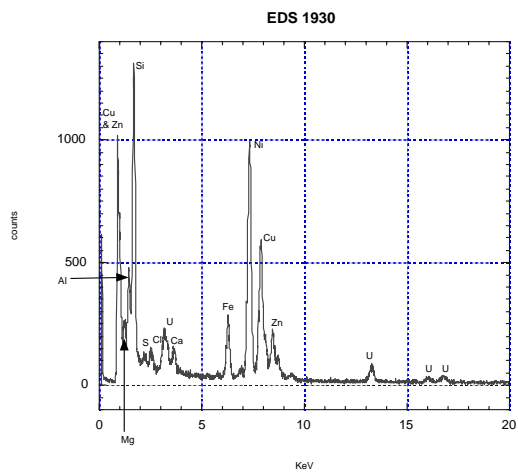
Block #	Grid #	Notebook Ref.	Digital Image Nos.	Comments and Elements Identified by EDS
NA	C433	SN1718:93	1957 1957diff 1957 center spot	Large amount of U and smaller amounts of O, Si, and Al. The 2 additional files are diffraction patterns. Diffraction data suggests the particles are UO ₂ .
NA	C433	SN1718:93	1958 1958 diff 1958 center spot 1958 combined	The diffraction data has been discarded due to using a camera length and exposure time that were too short. EDS shows a large amount of U & Si.
NA	C433	SN1718:93	1959 1959 diff 1959 center spot 1959 combined	Large amount of U and smaller amounts of O, Cl, and Si. The additional 3 files are diffraction patterns. Diffraction data suggests the particles are UO ₂ .



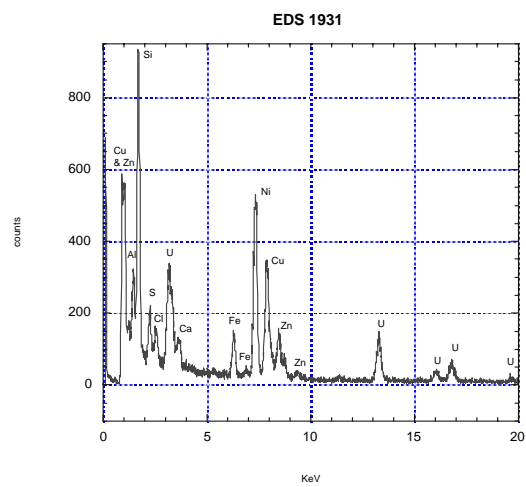
CCD 1930



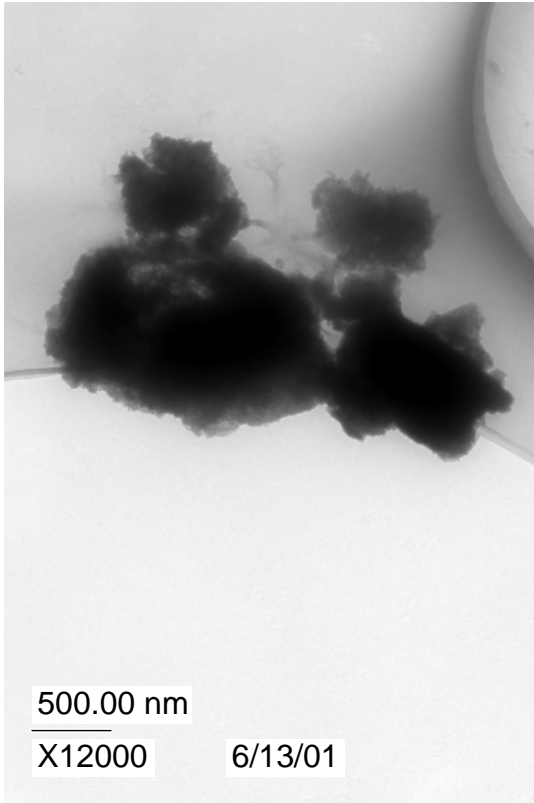
CCD 1931



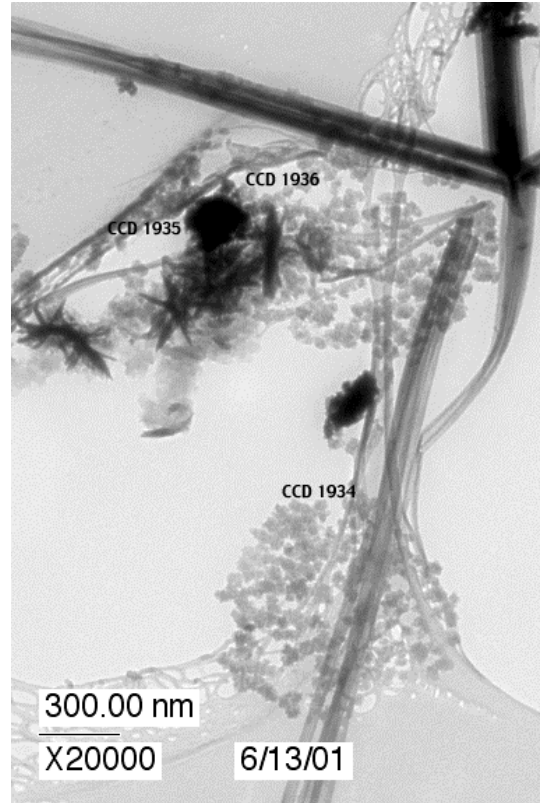
EDS of the Dark Material in CCD 1930



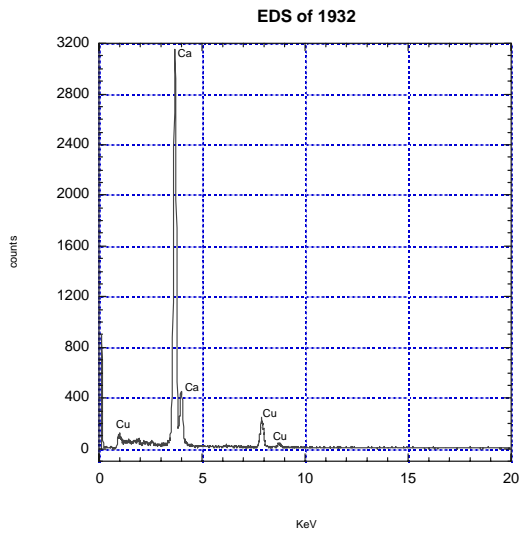
EDS of the Dark Material in CCD 1931



CCD 1932



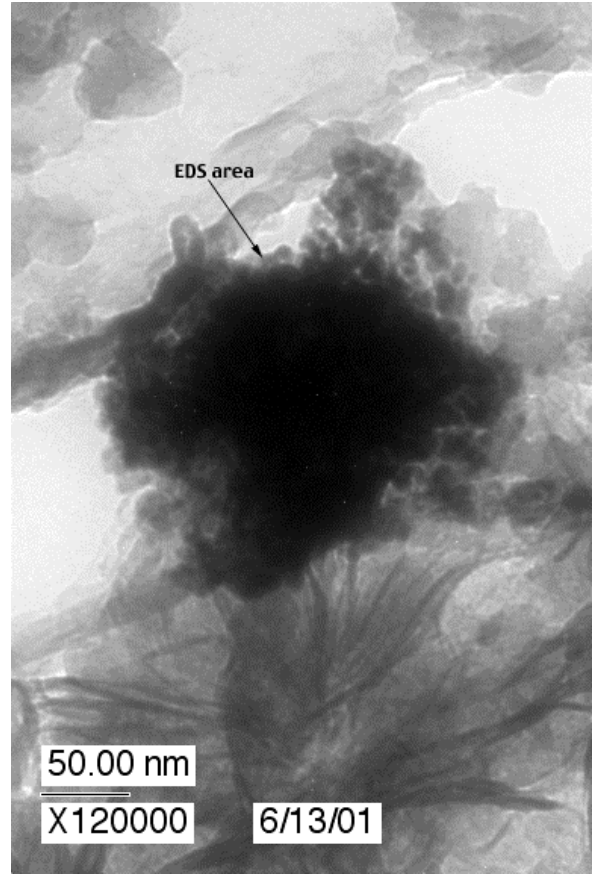
CCD 1933 - This is a low magnification overview image of the areas in CCD 1934, 1935 and 1936.



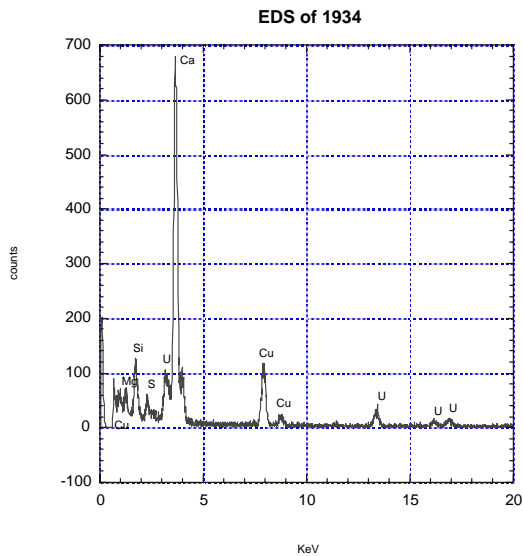
EDS of the Dark Particle in CCD 1932



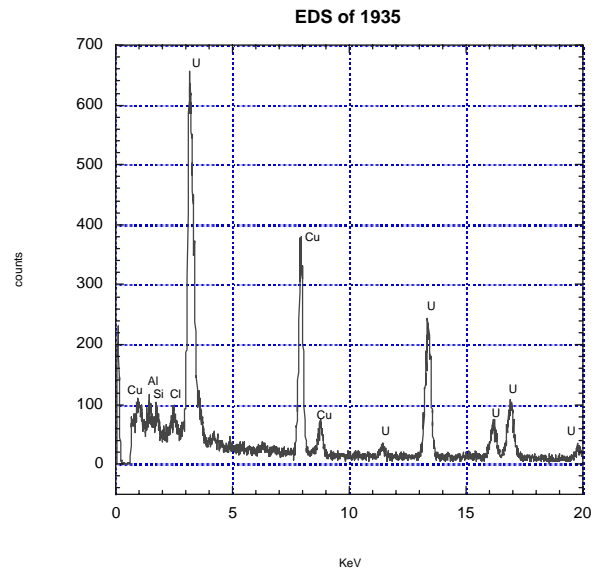
CCD 1934 - A High Magnification Image of the Indicated Area (the Light Round Material) in CCD 1933



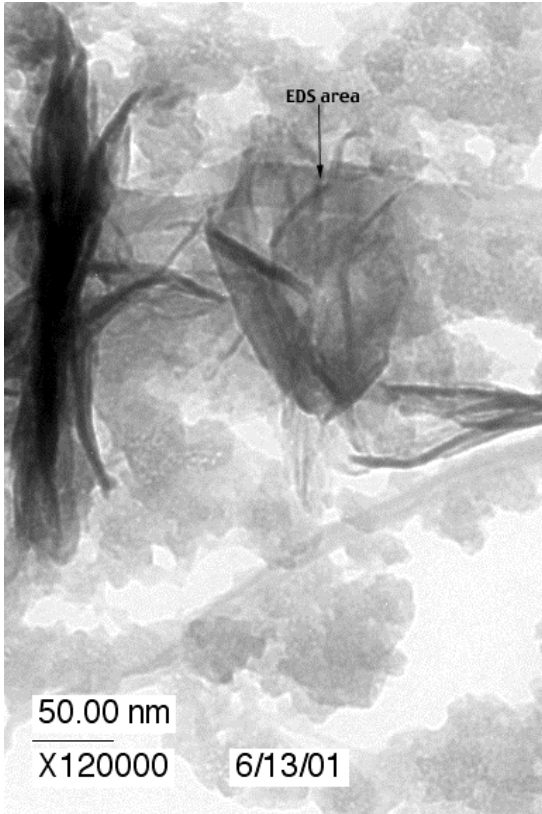
CCD1935 - A High Magnification Image of the Indicated Area (Dark Material) in CCD 1933



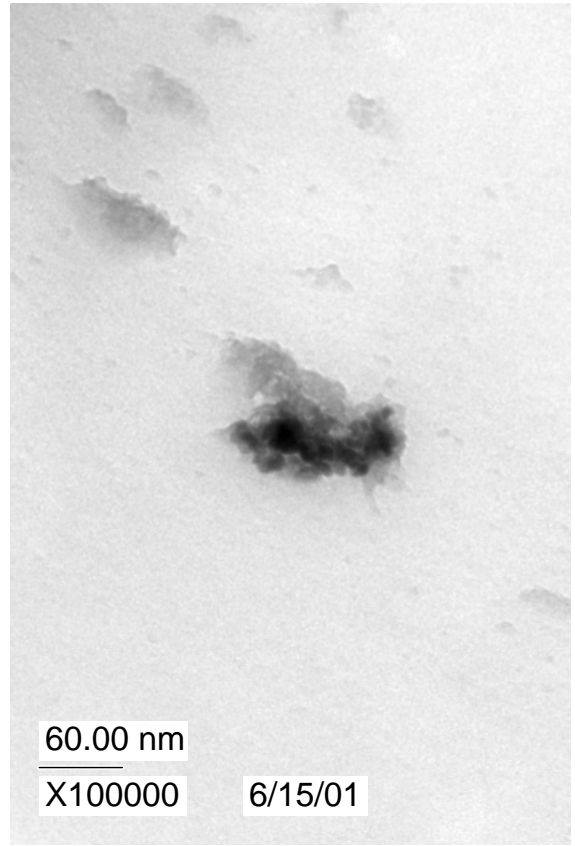
EDS of the Indicated Round Material in CCD 1934



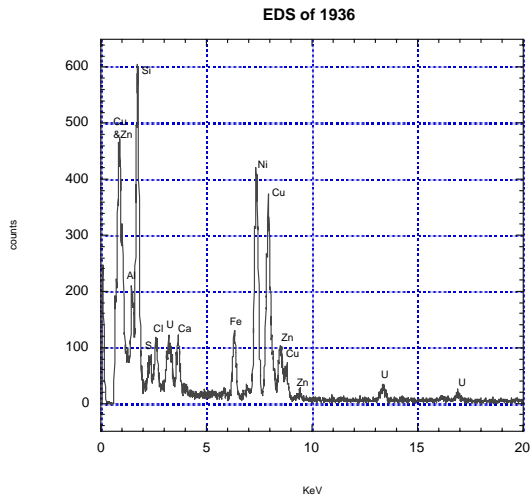
EDS of the Indicated Area in CCD 1935 (the Darkest Material)



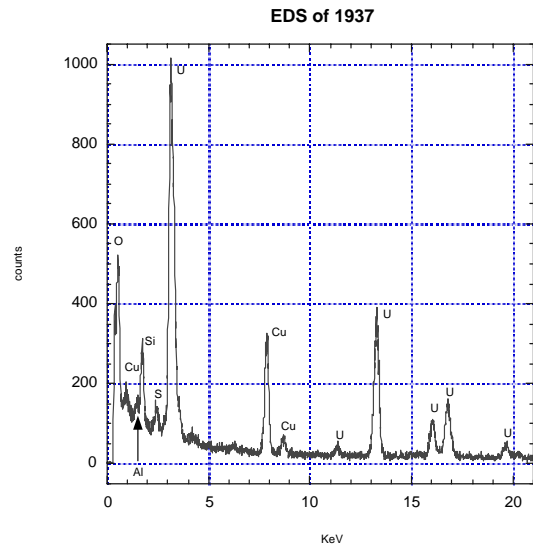
CCD 1936 - A High Magnification Image of the Indicated Area in CCD 1933



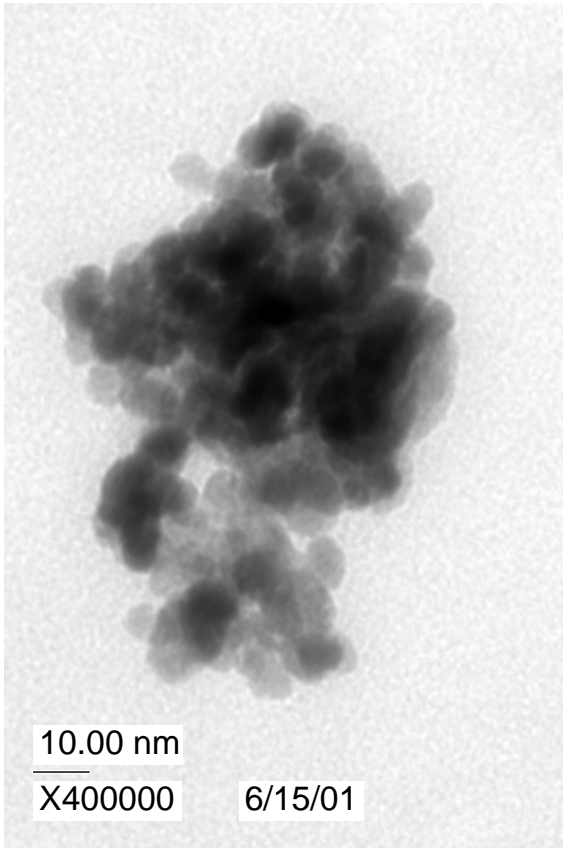
CCD 1937



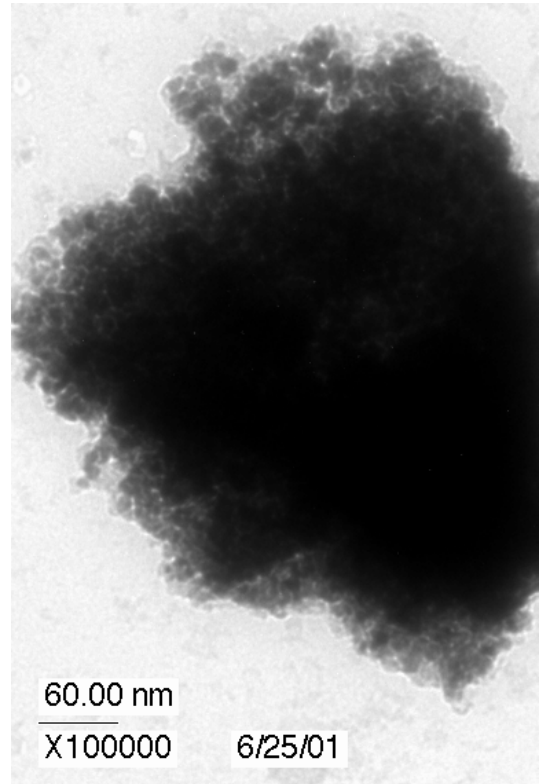
EDS of the Indicated Area in CCD 1936



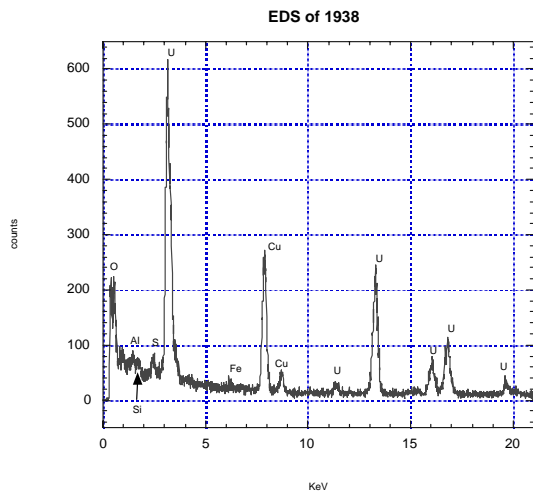
EDS of the Dark Material in the Center of CCD 1937



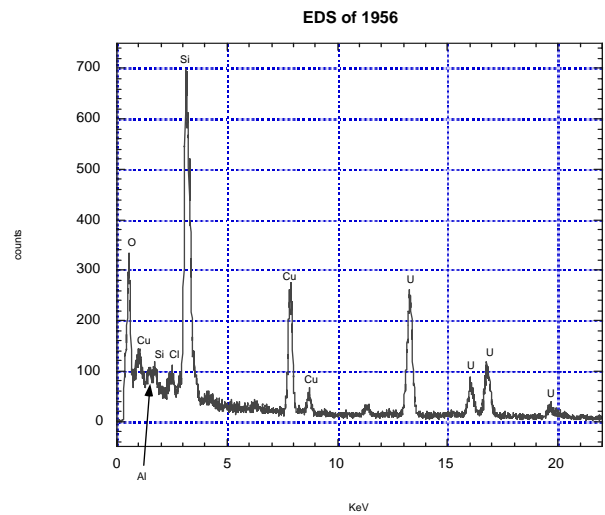
CCD 1938 - High Magnification Image Showing a Cluster of Particles in the 5-10 nm Size Range



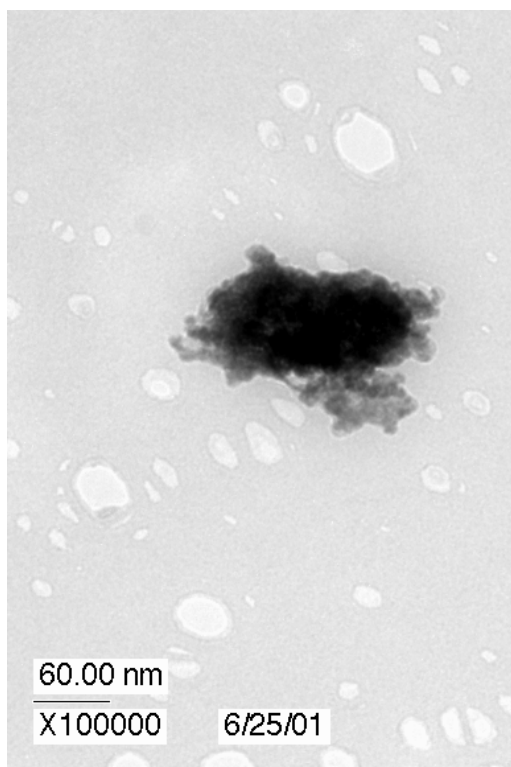
CCD1956 - A Large Area Rich in Si



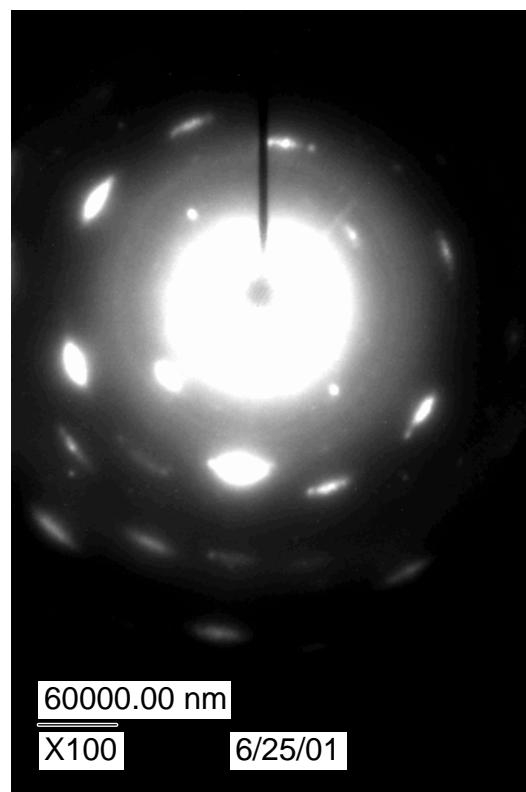
EDS of the Dark Round Material in CCD 1938



EDS of the Material in CCD 1956



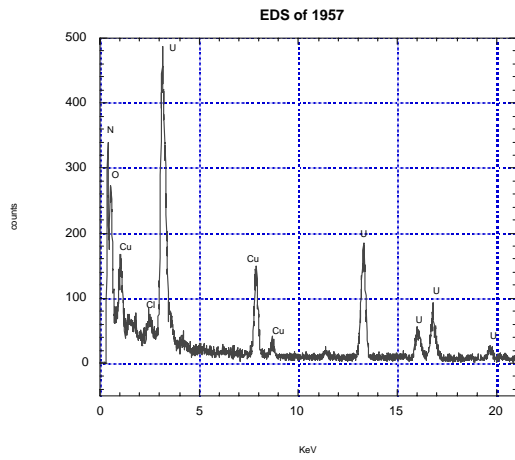
CCD 1957

Diffraction of the Material in CCD 1957
with the Center Spot Added and the
Brightness Enhanced

This diffraction data confirms that the material in CCD 1957 is UO_2 .

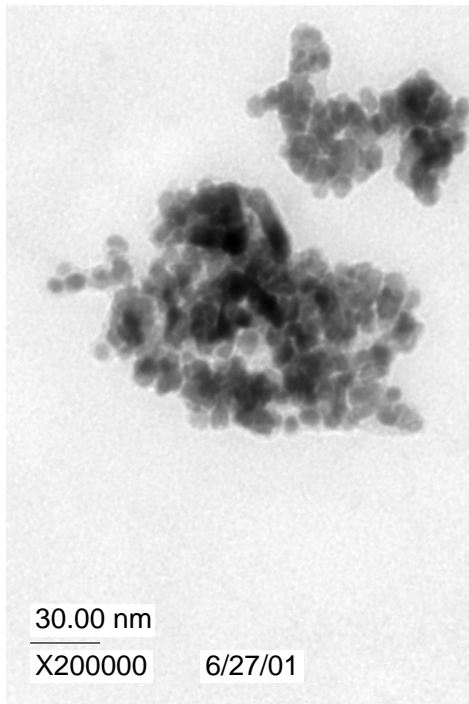
Diffraction from CCD Image k1957diff 100 Composite

Experimental 2Q ($1/\text{\AA}$)	Experimental d-spacing (\AA)	UO_2	$\text{UO}_{2.25}$
		JCPDS-ICDD 5-550 d-spacing (\AA)	JCPDS-ICDD 9-206 d-spacing (\AA)
		3.157	3.12
4.5	2.79	2.735	2.71
6.53	1.92	1.934	1.918
		1.649	1.636
		1.579	1.567
9.1	1.38	1.368	1.359
10.01	1.26	1.255	1.247
		1.223	1.215
		1.1163	1.11
11.73	1.07	1.0523	1.047
12.9	0.97	0.9666	

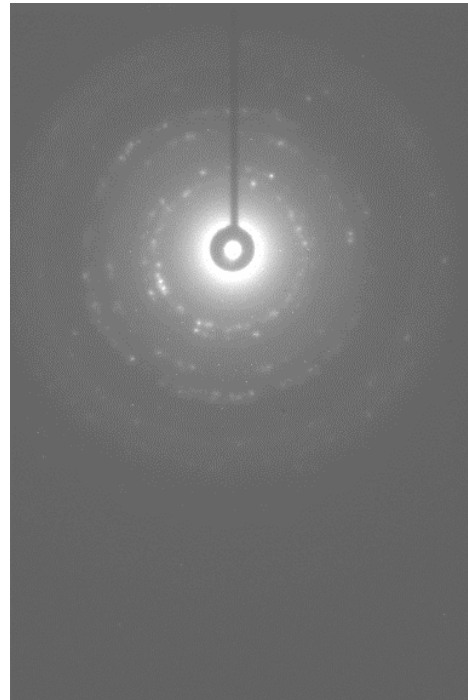


EDS of the Material in CCD 1957

Unfortunately, CCD 1958 and the associated diffraction patterns and EDS data was discarded due to excessively short exposure times and camera length.



CCD 1958

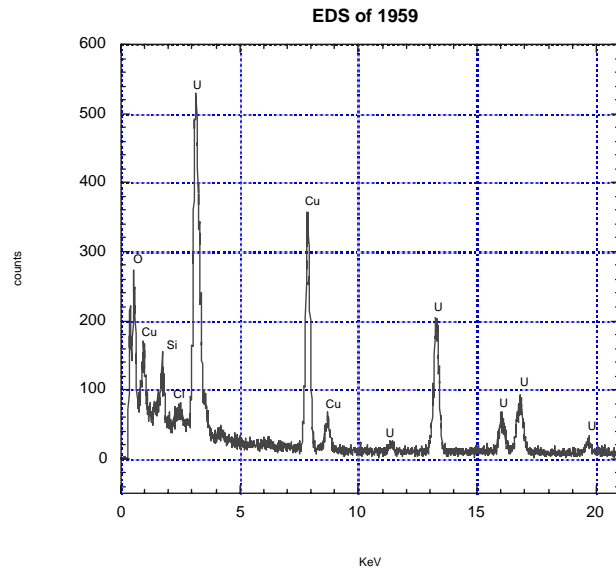


This is the diffraction pattern from the particles in CCD 1959 with the addition of the center spot to the pattern.

The diffraction data suggests a systematic shift but does confirm that the particles in CCD 1959 are UO_2 .

Diffraction from CCD Image k1957diff 100 Composite

Experimental 2 θ ($1/\text{\AA}$)	Experimental d-spacing (\AA)	UO_2	$\text{UO}_{2.25}$
		JCPDS-ICDD 5-550 d-spacing (\AA)	JCPDS-ICDD 9-206 d-spacing (\AA)
4.14	3.04	3.157	3.12
4.93	2.55	2.735	2.71
6.52	1.93	1.934	1.918
		1.649	1.636
7.99	1.57	1.579	1.567
9.53	1.32	1.368	1.359
10.59	1.19	1.255	1.247
		1.223	1.215
		1.1163	1.11
11.79	1.06	1.0523	1.047
		0.9666	



EDS of the Material in CCD 1959

Distribution for ANL-01/33Internal:

J. C. Cunnane
N. M. Dimitrijevic
W. L. Ebert
R. E. Einziger
P. A. Finn

J. A. Fortner
M. M. Goldberg
M. D. Kaminski (20)
D. Lewis
C. J. Mertz

R. T. Riel
Y. Vojta
TIS File

External:

DOE-OSTI
ANL-E-Library
ANL-W-Library

Chemical Technology Division Review Committee Members:

H. U. Anderson, University of Missouri-Rolla, Rolla, MO
A. L. Bement, Jr., Purdue University, West Lafayette, IN
R. A. Greenkorn, Purdue University, West Lafayette, IN
C. L. Hussey, University of Mississippi, University, MS
M. V. Koch, University of Washington, Seattle, WA
V. P. Roan, Jr., University of Florida, Gainesville, FL
J. R. Selman, Illinois Institute of Technology, Chicago, IL
J. S. Tulenko, University of Florida, Gainesville, FL
M. Ebner, Idaho National Environmental and Engineering Lab, Idaho Falls, ID
H. H. Loo, Idaho National Environmental and Engineering Lab, Idaho Falls, ID
C. Shelton-Davis, Idaho National Engineering and Environmental Laboratory,
Idaho Falls, ID